FIRST SEMI-ANNUAL REPORT

NASA Research Grant NAG 8-684

Period of Performance
10-1-87 through 4-1-88

ANALYSIS OF LOW GRAVITY TOLERANCE OF MODEL EXPERIMENTS FOR SPACE STATION: PRELIMINARY RESULTS FOR DIRECTIONAL SOLIDIFICATION

J. IWAN D. ALEXANDER AND JALIL OUAZZANI

Center for Microgravity and Materials Research
The University of Alabama in Huntsville
Huntsville, Alabama 35899

TABLE OF CONTENTS

1 INTRODUCTION

It has become clear from measurements of the acceleration environment in the Spacelab [1,2] that the residual gravity levels on board a spacecraft in low earth orbit can be significant and should be of concern to experimenters who wish to take advantage of the low gravity conditions on future Spacelab missions and on board Space Station. While accelerations may be orders of magnitude lower than that experienced at the earth's surface, they are nonetheless finite and pose potential problems for certain types of experiment, particularly those for which minimization of accelerations is desirable. Motivated by the need to further our understanding of the effects of residual accelerations on materials science experiments we have embarked upon a research program, funded by NASA, entitled "*Process Modelling for Space Station Experiments* ". The basic goals of the program are to better understand the low-gravity tolerance of three classes of materials science experiments: Crystal growth from a melt, a vapor and a solution. Each class of experiment is represented by one or more "generic" numerical models which incorporate the essential elements of the mass, heat and momentum transport mechanisms associated with each process. The results of the research will provide guidance toward the determination of the sensitivity to the low-gravity environment, the design of the laboratory facilities and the timelining of materials science experiments.

To date, analyses of the effects of the microgravity environment have, with a few exceptions [3-5], been restricted to order of magnitude estimates [6-9]. The validity of the various estimates has only been demonstrated for a few special cases [10] and we have found that some techniques used to estimate the response to residual gravity are liable to be grossly inaccurate.

In this communication we report preliminary results obtained from numerical models of the effects of residual steady and time dependent acceleration on

1) heat, mass and momentum transport during the growth of a dilute alloy by the Bridgman-Stockbarger technique

2) the response of a simple fluid physics experiment involving buoyant convection in a square cavity.

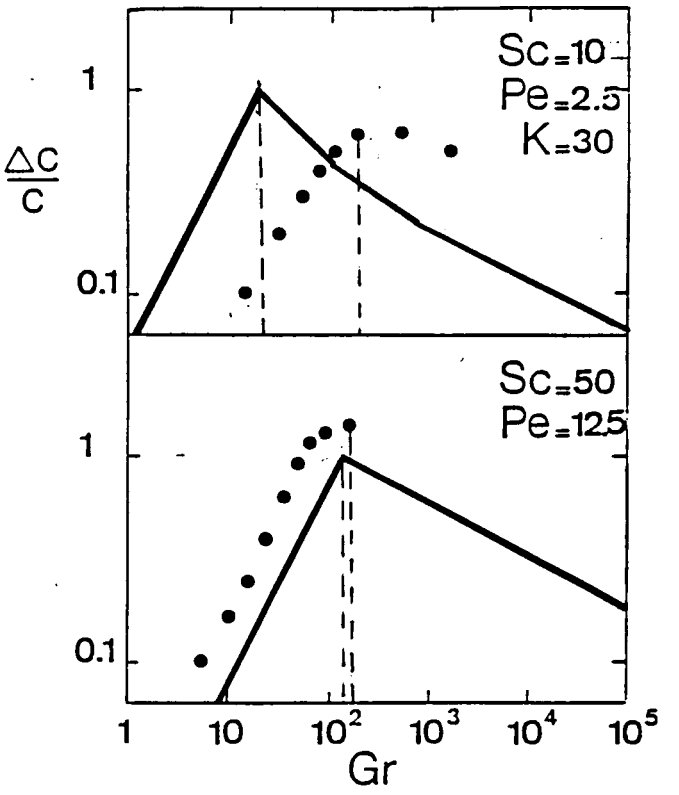

Figure 1. Grashof number dependence of convection induced radial non-uniformity in Ga concentration in a Ge crystal growing from the melt. Comparison of *a priori* estimates with numerical simulations [16]. (After Camel and Favier [15].)

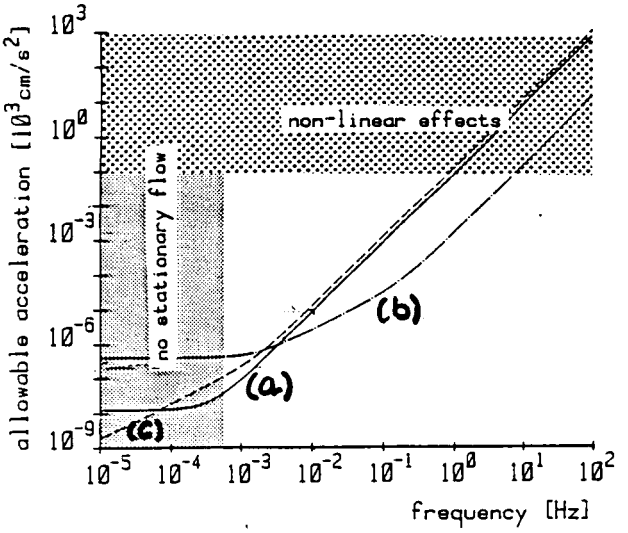

Figure 2 a. Tolerable residual accelerations for (a) a fluid physics experiment involving a temperature gradient, (b) a crystal growth experiment, (c) a thermo-diffusion experiment.

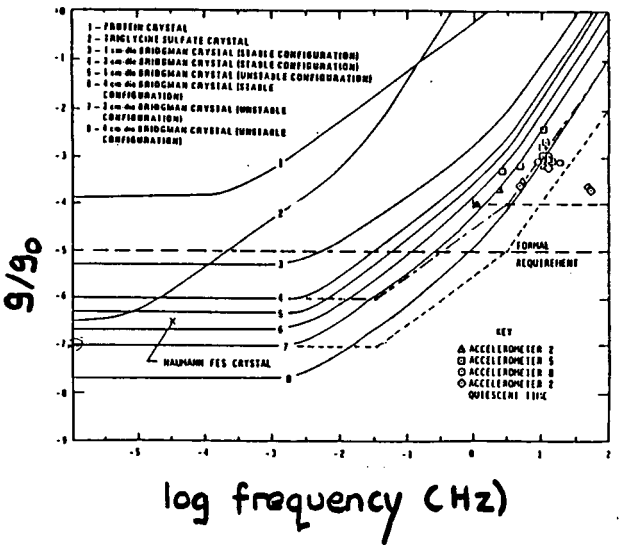

Figure 2 b. G-level tolerance for single frequency disturbances.

Comparison of our results with the current "g-level" requirement for the Space Station [11], suggests that the requirements would be adequate for these experiments for the specific dimensions and operating conditions investigated.

2 SUMMARY OF PREVIOUS WORK

2.1 ORDER OF MAGNITUDE ESTIMATES

To date, g-tolerance levels for a variety of processes have been estimated by Langbein and Tiby [6], Favier et al. [7,9] and Monti and Napolitano [5,12]. Their work is summarized in a recent review article [9]. Probably the most refined methods of constructing order of magnitude estimates of the effects of low-gravity levels on materials processing experiments are those developed by Camel and Favier [13-15]. These methods attempt to arrive at an appropriate choice of physical length scale, which is a crucial factor in determining the fidelity of the estimate. The importance of length scales is highlighted by the failure of the Langbein-Tiby approach (which neglects the need for an appropriate choice of length scale) to agree with our calculated results (see **Section 4**) and those obtained by others. Indeed, their estimates overestimated the effects of *steady* low-gravity by several orders of magnitude. It should be pointed out, however, that an appropriate choice of length scale for the situation they examined is not readily determined. This is true for many other situations. In view of the typically three-dimensional nature of the transport environment and the large disparity in transport coefficients for heat, mass, momentum and species in the systems of technological interest, the problem remains that an *a priori* choice of length or time scales may not be obvious. For example, the estimates of Rouzaud et al. [10] and Camel and Favier [15] are in reasonable agreement with the calculations of Chang and Brown [16] for a Schmidt number of fifty (see figure 1) but overestimate the amount of radial segregation for a Schmidt number of ten.

For time-dependent disturbances estimates of the response of a system to a "monochromatic" or single frequency variation in residual g-level (see figure 2 for typical results). Since, in general, the microgravity environment is not characterized by a single frequency disturbance the

"g-tolerance curves" may be misleading if the system displays an additive response, or a resonant frequency is excited. An example of the additive effect of a multiple component disturbance is that of the DMOS experiment [17] which flew on STS-61-B. The post flight analysis has demonstrated that the amount of mixing observed between organic liquids can be explained by the additive response of the system to a multicomponent disturbance. It should be emphasized, however, that the response of a system to a disturbance consisting of several frequencies will, in general, not be equivalent to the sum of the responses of that same system to the component single frequency disturbances. Reasons for this departure from linearity are discussed in **Section 3.**

2.2 NUMERICAL MODELS

The effects of low gravity on the transport of heat and momentum have been examined by Robertson et al. [18,19] Spradley et al. [20] and Kamotani and Ostrach [3]. Robertson et al. found that for convection in circular cylinders with azimuthal variations in temperature at the boundary and the gravity vector applied perpendicular to the cylinder axis, the intensity of convection follows the prediction of Weinbaum's first order theory[1] [21] for low Rayleigh numbers. Spradley et al. [20] examined the effect of a variety of acceleration vectors. They found that if the applied disturbance is decomposed into a steady mean part and an oscillatory part, the steady mean part is more important than the oscillatory part in determining the flow field and heat transfer rate. Kamotani and Ostrach [3] solved a linearized approximation of the Boussinesq equations, and investigated the effect of an applied acceleration consisting of a time mean part and an oscillatory part on the temperature and flow fields in a rectangular enclosure. They found that the thermal convection was predominantly oscillatory in nature.

McFadden and Coriell [4] have undertaken 2-D calculations of the effects of time-dependent accelerations on lateral compositional variations during directional solidification. The gravitational acceleration was assumed to have a uniform magnitude and rate of rotation. The degree of

---

[1] Weinbaum's first order theory predicts a simple sinusoidal dependence of the maximum velocity as a function of orientation of the gravity vector.

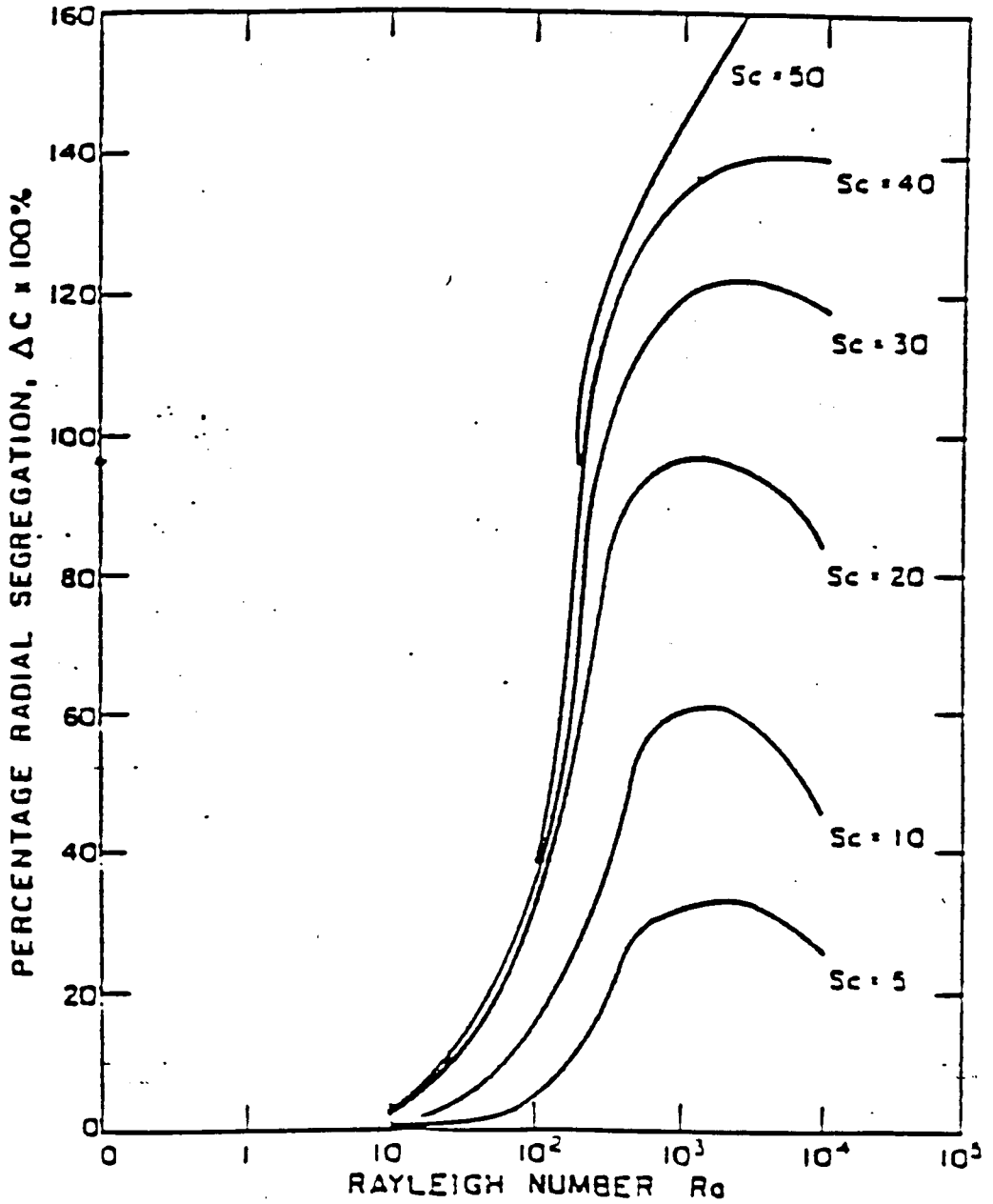

Figure 3. Compositional non-uniformity as a function of Rayleigh number, for Schmidt numbers in the range 10 - 50. (After Chang and Brown [16].)

compositional non-uniformity was found to increase with increasing period (angular rate of rotation).

In order to improve our understanding of the physics of heat and mass transport, and to investigate the extent to which the order of magnitude estimates can be relied upon to predict the low gravity tolerance levels, we have developed numerical models of "generic" experiments and examined them under a variety of specific low gravity conditions. We have found that the degree to which a fluid system responds to variations in the residual acceleration depends not only on the physical properties of the fluids, but that the nature of that response (particularly the effect on heat and solute transport) is strongly dependent on the nature of the thermal boundary conditions of the system.

In this report we describe the preliminary results of our work which focuses on a generic model of directional solidification by the Bridgman technique. The model is based upon the pioneering work of Chang and Brown [16] involving (axisymmetric) numerical simulations of steady directional solidification in a Bridgman configuration. Through a systematic variation of the Rayleigh number they found that the sensitivity of radial solute segregation to melt convection is such that it reaches a maximum at intermediate values of the Rayleigh number (see figure 3). Thus in order to be an effective processing parameter the degree to which the acceleration is reduced must be sufficient to avoid such solute transport regimes.

In the following sections we formulate the basic model, define the range of operating conditions under consideration and consider the effect on solute redistribution of a variety of orientations of steady and time-dependent acceleration vectors.

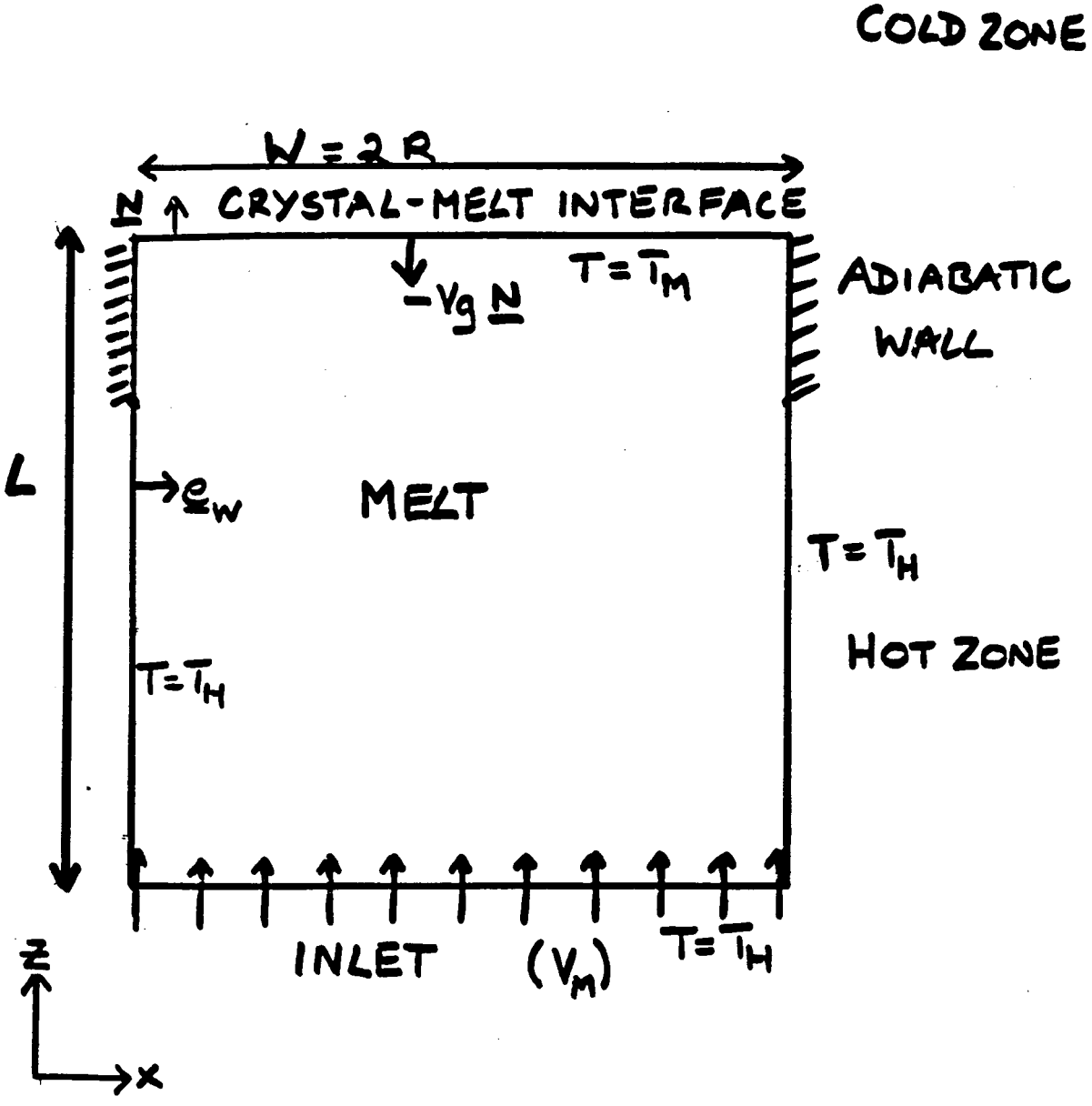

Figure 4. Sketch defining our prototype model for directional solidification

3. STEADY AND TIME-DEPENDENT LOW GRAVITY: EFFECT ON TRANSPORT CONDITIONS DURING DIRECTIONAL SOLIDIFICATION BY THE BRIDGMAN TECHNIQUE.

3.1 FORMULATION OF THE MODEL

As a first attempt to model the effect of residual accelerations on crystal compositional uniformity during directional solidification by the Bridgman-Stockbarger technique we adopted and modified the basic model advanced in Chang and Brown's [16] pioneering work. The basic attributes of our two-dimensional and three-dimensional models are as follows.

Directional solidification takes place as an ampoule is translated through fixed "hot " and "cold" zones. The zones are separated by a thermal barrier which is modelled using adiabatic sidewalls. The temperature conditions are chosen such that the upper and lower parts of the system are solid and molten respectively. Translation of the ampoule is modelled by supplying a melt at a constant velocity V_m and a dilute bulk composition c_∞ at the bottom of the computational space considered. The crystal-melt interface is located at a distance L from the bottom of the computational space and advances at a rate $V_g = V_m(\rho_m/\rho_s)$ where ρ_m and ρ_s are the melt and crystal densities, respectively. The temperature at the interface is taken to be T_M the melting temperature of the crystal, while the lower boundary is held at a temperature T_H. In an actual experiment, owing to the finite length of the ampoule there is a gradual decrease in length of the melt zone. In this model transient effects related to this change are ignored. Thus, it is assumed that the ampoule is sufficiently long for these effects to be negligible. The only transient effects to be considered will arise directly from the time dependent nature of the residual gravity field. We also assume that the contribution of the solute to convection is negligible. Convection is driven only by thermal gradients.

The governing equations are cast in dimensionless form using L, κ/L (where κ is the melt's thermal diffusivity), $\rho_m\kappa^2/L^2$, T_H-T_M, and c_∞ to scale the lengths, velocity, pressure, temperature and solute concentration respectively.

TABLE 1

Typical forms of the acceleration vector examined in this work.

Steady

$\mathbf{g}_o = g_{ox}\,\mathbf{i} + g_{oz}\,\mathbf{k}$;

$||\mathbf{g}|| = \sqrt{2}(10)^{-5}$, $5\sqrt{2}(10)^{-6}$, $\sqrt{2}(10)^{-6}$, $\sqrt{2}(10)^{-7}$

Time dependent

$\mathbf{g}(t) = \mathbf{g}_o + \mathbf{g}_n \cos(2\pi\omega_n t)$; $\mathbf{g}(t) = \mathbf{g}_o + \Sigma\, \mathbf{g}_n \cos(2\pi\omega_n t)$;

$\omega_n = 10^{-4}$, 10^{-3}, 10^{-2}, 10^{-1}, 1, 10 Hz,

$||\mathbf{g}_n|| = \sqrt{2}(10)^{-5}$, $5\sqrt{2}(10)^{-6}$, $\sqrt{2}(10)^{-6}$

Impulse

$$\mathbf{g}(t) = \begin{cases} \sqrt{2}(10)\text{-}6, & t < t_1\ ,\ t > t_2 \\ 3\sqrt{2}(10)\text{-}3, & t_1 < t < t_2 \end{cases}$$

For the two dimensional model a dilute binary melt is assumed to occupy a rectangular region Ω which is bounded at z= 0 and z= 1 by planar surfaces (see figure 4). In the three dimensional model the rectangular region is replaced by a circular cylinder with a dimensionless radius R = 0.5.

The dimensionless equations governing momentum, heat and solute transfer in the melt are

$$\frac{\partial \mathbf{u}}{\partial t} + (\text{grad } \mathbf{u})\mathbf{u} = -\text{grad}p + Pr\Delta \mathbf{u} + RaPr\,\theta \mathbf{g}(t), \quad (1)$$

$$\text{div } \mathbf{u} = 0, \quad (2)$$

$$\frac{\partial \theta}{\partial t} + \mathbf{u} \cdot \text{grad}\,\theta = \Delta \theta, \quad (3)$$

$$\frac{Sc}{Pr}\left(\frac{\partial C}{\partial t} + \mathbf{u} \cdot \text{grad}\,C\right) = \Delta C, \quad (4)$$

where, $\mathbf{u}(\mathbf{x},t)$ represents the velocity, $\theta = (T(\mathbf{x},t) - T_M)/(T_H - T_M)$ the temperature (where $T_H - T_M$ is the temperature difference between the hot zone and the crystal interface) and C represents the solute concentration. The parameters $Pr=\nu/\kappa$, $Ra= g\beta(T_H-T_M)L^3/\kappa$ and $Sc=\nu/D$ are respectively the Prandtl, Rayleigh and Schmidt numbers. The term $\mathbf{g}(t)$ in equation (1) represents the time-dependent gravity vector. The value of g in Ra is taken to be 980 cm s^{-2}, i.e. equal to the terrestrial acceleration. Thus, the magnitude of $\mathbf{g}$ represents the ratio between the actual residual acceleration and g. Table 1 lists the forms of $\mathbf{g}(t)$ we have examined to date.

The following boundary conditions apply at the crystal-melt interface

$$\theta = 0, \quad (5)$$

$$\mathbf{u} \cdot \mathbf{N} = Pe/\sigma, \quad (6)$$

$$\mathbf{N} \times \mathbf{u} \times \mathbf{N} = \mathbf{0}, \quad (7)$$

$$\frac{\partial C}{\partial z} = \frac{PeSc}{Pr}(1-k)\,C, \quad (8)$$

where $\mathbf{N}$ points into the crystal and is the unit vector perpendicular to the planar crystal melt interface, and , $\sigma = \rho_m/\rho_s$ and k is the distribution

TABLE 2

Dimensionless parameters and representative values for gallium-doped germanium system

Group	Definition	Value
Rayleigh number	$Ra = \beta g(T_M - T_m)L^3/\alpha_L \nu$	$0-10^7$
Prandtl number	$Pr = \nu/\alpha_L$	0.01
Péclet number	$Pe = V_S L/\alpha_L$	0.005
Conductivity ratio	$K = k_S/k_L$	1.0
Stefan number	$S = \Delta H_f/\rho_L c_{p_L}(T_h - T_c)$	1.0
Schmidt number	$Sc = \nu/\mathcal{D}$	10
Thermal diffusivity ratio	$\gamma = \alpha_S/\alpha_L$	1.0
Density ratio	$\sigma = \rho_S/\rho_L$	1.0

Material properties characteristic of gallium-doped germanium

Property	Value
Thermal conductivity of melt (k_L)	0.17 W/K·cm
Thermal conductivity of solid (k_S)	0.17 W/K·cm
Heat capacity of melt (c_{p_L})	0.39 J/g·K
Heat capacity of solid (c_{p_S})	0.39 J/g·K
Density of melt (ρ_L)	5.6 g/cm^3
Density of solid (ρ_S)	5.6 g/cm^3
Melting teperature (T_m)	958°C
Kinematic viscosity of melt (ν)	1.3×10^{-3} cm^2/s
Heat of fusion (ΔH_S)	506 J/g
Thermal expansion coefficient (β)	0.25×10^{-3} K^{-1}
Diffusivity of Ga in Ge ($\mathcal{D}$)	1.3×10^{-4} cm^2/s
Segregation coefficient of Ga in Ge (k)	0.1

coefficient. We define the measure of compositional non-uniformity in the crystal at the interface to be

$\xi = (C_{max} - C_{min})/k = (c_{smax} - c_{smin})/c_\infty$,

where c_s is the (dimensional) solute concentration in the crystal.

At the "inlet" (z=0) the following boundary conditions are applied

$$\frac{\partial C}{\partial z} = \frac{PeSc}{Pr}(C-1), \tag{9}$$

$$\theta = 1, \tag{10}$$

$$\mathbf{u}\cdot\mathbf{N} = Pe\sigma, \tag{11}$$

$$\mathbf{N}\times\mathbf{u}\times\mathbf{N} = \mathbf{0}, \tag{12}$$

Equations (8) and (9) express conservation of mass at the crystal-melt interface and the "inlet" respectively. Equations (6) and (10) guarantee continuity of the melt with the crystal and with the supply of melt at the "inlet", while equations (7) and (11) ensure no-slip tangent to the interface and the top surface. At the side walls the following conditions are applied

$$\mathrm{grad}\, C\cdot\mathbf{e}_w = 0, \qquad \mathbf{u}\cdot\mathbf{N} = Pe\sigma, \quad \mathbf{e}_w\cdot\mathbf{u} = 0, \tag{13}$$

along with

$$\theta = 1, \tag{14}$$

in the isothermal zone and

$$\mathrm{grad}\,\theta\cdot\mathbf{e}_w = 0, \tag{15}$$

in the adiabatic zone. Here $\mathbf{e}_w$ is the outward pointing normal to the ampoule wall.

While the above model does not strictly apply to a specific furnace (for example details of the heat transfer at the ampoule walls are neglected), it nonetheless serves as a reasonable "generic" model with which to carry out a preliminary analysis of a directional solidification experiment under conditions characteristic of the low gravity environment of space.

Our calculations are limited to thermo-physical properties corresponding to the system gallium-doped germanium (Ga:Ge). The definitions and values of the dimensionless groups and the associated

thermo-physical properties are given in Table 2. For all our calculations the length, L, of the furnace and the temeperature difference T_H - T_M were taken to be 1 cm and 115° C, respectively.

3.2 METHOD OF SOLUTION

The governing equations were solved using the code PHOENICS [22]. PHOENICS embodies a finite volume or finite domain formulation [23]. This method first involves the discretization of the governing equations (expressed in conservation form) within finite control volumes or cells. Within each of these topologically Cartesian volumes a "grid node" is identified. The grid node may be thought of as a point within the volume at which the fluid properties are representative of the whole volume. The fluid properties are interpolated from the cell boundary to the interior. The discretized differential equations are then integrated over the control volume. After this procedure has been completed for the entire computational domain a set of "finite domain equations" results. These are solved iteratively using a tri-diagonal matrix algorithm (TDMA) i.e. an alternating direction implicit (ADI) method. For the 2-D calculations discussed in this report we employed a 40x39 grid. The 3-D calculations were performed in a circular cylindrical domain with 20 nodes in the radial direction, 12 in the azimuthal direction and 39 in the axial direction. We found that for the 2-D calculation less than 40 points in the direction parallel to the interface resulted in poor convergence of the solute field. A Tchebyshev mesh was employed in the direction perpendicular to the interface which improves resolution and furthermore admits the use of a spectral operator[2] to solve the solute fields. The addition of a subroutine with a spectral operator results in faster accurate calculations at higher values of the Schmidt number.

The scheme employed has the same accuracy as a finite difference scheme which is of the order Δx, where Δx is the distance between the grid nodes. The time scheme is implicit and thus unconditionally stable. However, small time steps are required to obtain accurate solutions. For

[2] A spectral method which can be used as a PHOENICS subroutine has been developed at the CMMR .

highly non-linear flows the use of under-relaxation is necessary to eliminate divergence and to ensure good convergence of the solutions.

The mixed Neumann-Dirichlet boundary conditions at the inlet and the crystal melt interface have the form

$$\frac{\partial C}{\partial z} + \beta C = 0, \tag{16}$$

where β is a constant. This class of conditions is better handled via the transformation (particularly when β is large):

$$s = \ln C. \tag{17}$$

Then

$$\frac{\partial C}{\partial z} \rightarrow \exp(s)\frac{\partial s}{\partial z}, \quad C \rightarrow \exp(s), \tag{18}$$

and (16) becomes

$$\frac{\partial s}{\partial z} + \beta = 0. \tag{19}$$

Thus solute transport equation (4) is transformed to

$$\frac{Sc}{Pr}\left(\frac{\partial s}{\partial t} + \mathbf{u} \cdot \operatorname{grad} s\right) = \Delta s + \operatorname{grad} s \cdot \operatorname{grad} s. \tag{20}$$

Having solved for s, C can be obtained from (17).

In order to test our codes we compared our calculations (to be discussed in detail in the following sections) with the results of Chang and Brown axisymmetric calculations [16]. Our 3-D computations were found to be in agreement with their work. For Rayleigh numbers of 6.25 and greater (corresponding to Ra > 100 in [16]) the two dimensional radial segregation predictions were approximately 10% higher than obtained from our three dimensional calculations. In addition we carried 3-D non-axisymmetric steady calculations in order to calibrate our 2-D results. For one set of examples we found that with $\sqrt{2}\ (10)^{-5}$g parallel to the interface the percentage compositional uniformity predicted by the 2-D calculation (ξ = 152%) was twice that predicted by the full 3-D calculation. This difference is mainly due to the fact that the solute is redistributed azimuthally as well as laterally. A comparison between 2-

and 3-D calculations for $\sqrt{2}(10)^{-6}$ g revealed that there was no significant difference in ξ between the 2-D and 3-D calculations.

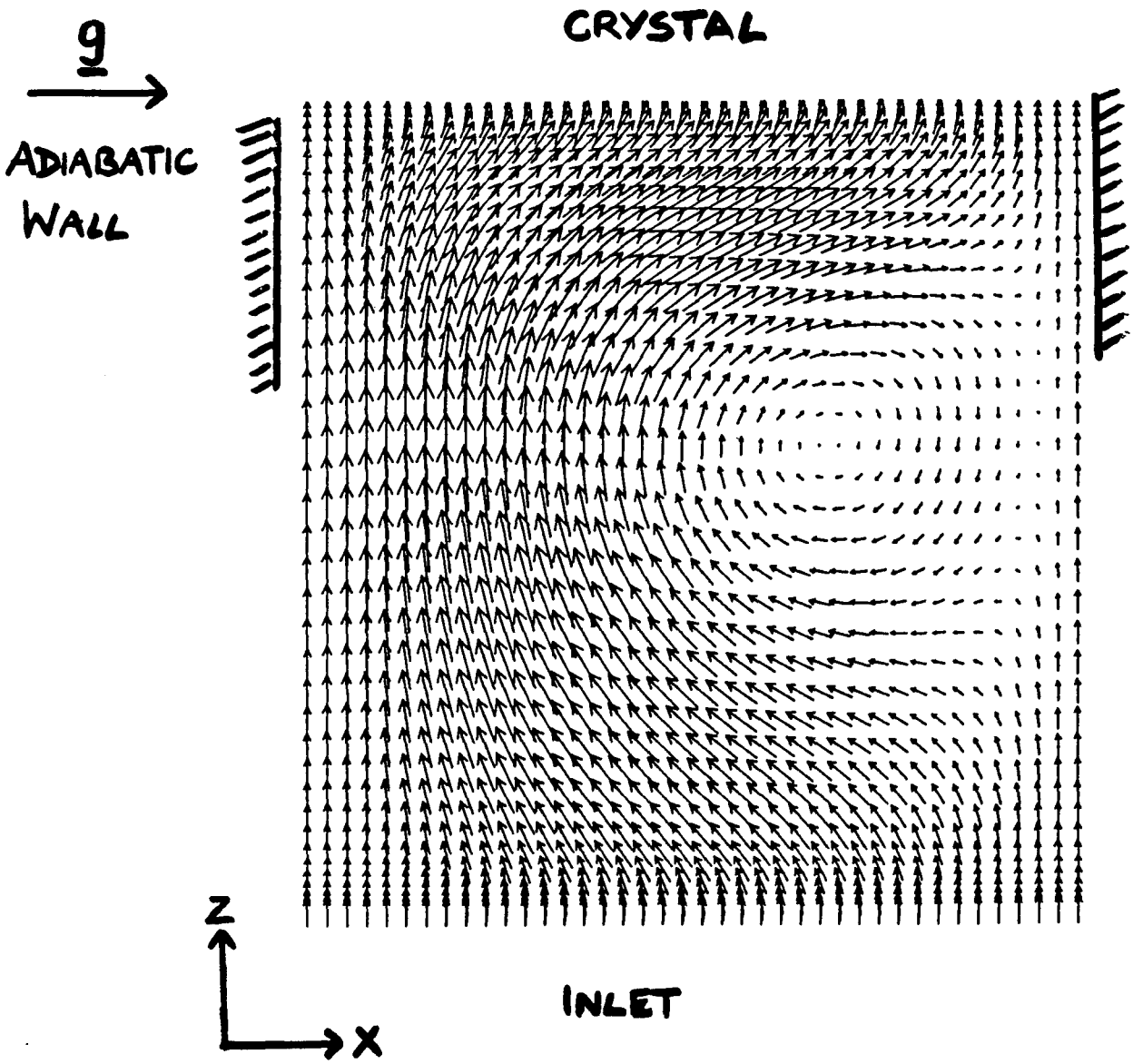

Figure 5. The steady flow field produced by a residual acceleration with a magnitude $\sqrt{2}(10)^{-5}$ g acting parallel to the crystal melt interface. The maximum speeds are approximately twice the growth speed, $V_g = 6\ \mu m\ s^{-1}$.

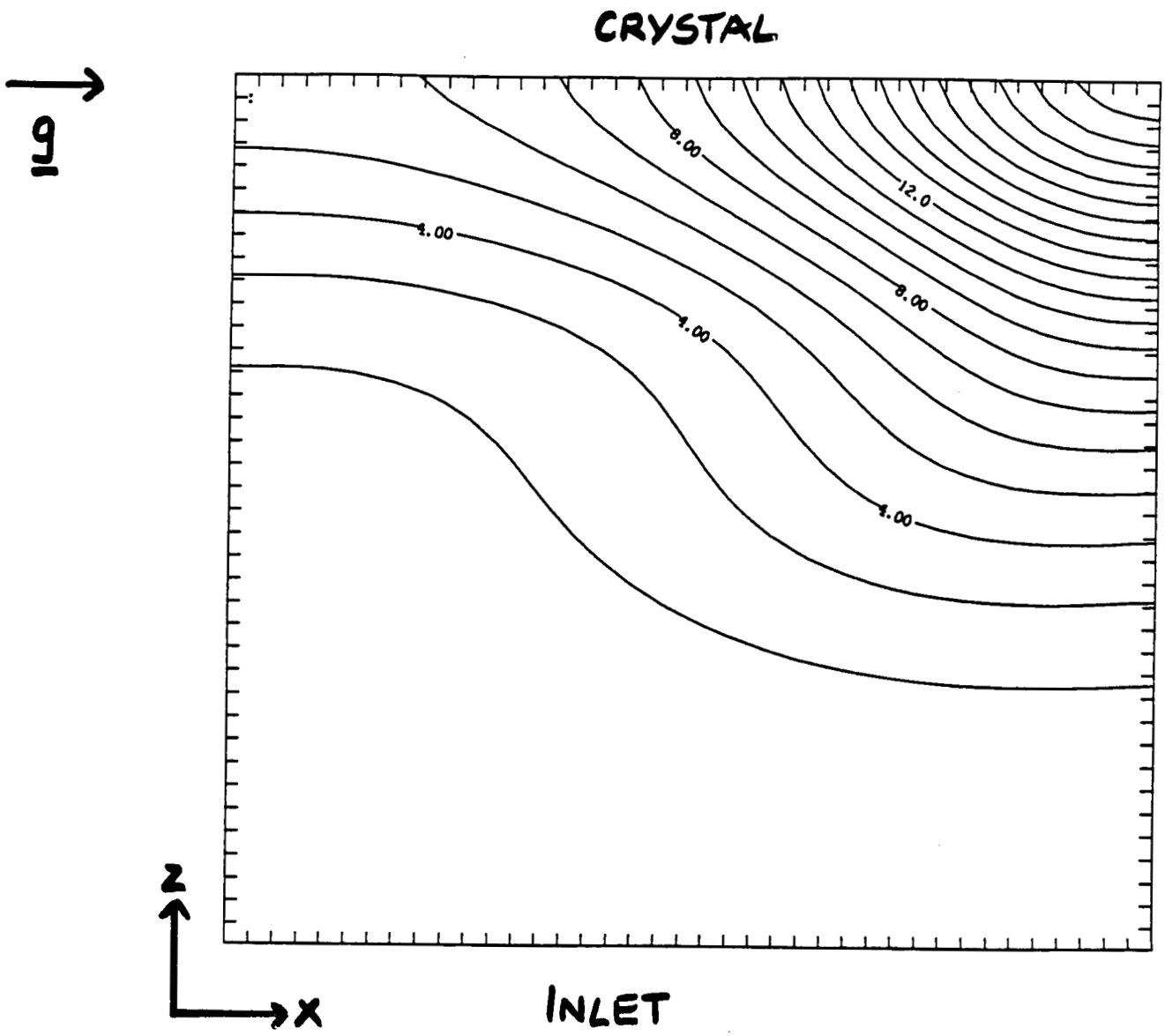

Figure 6. The solute field associated with the flow depicted in figure 5. For this case ξ= 152%.

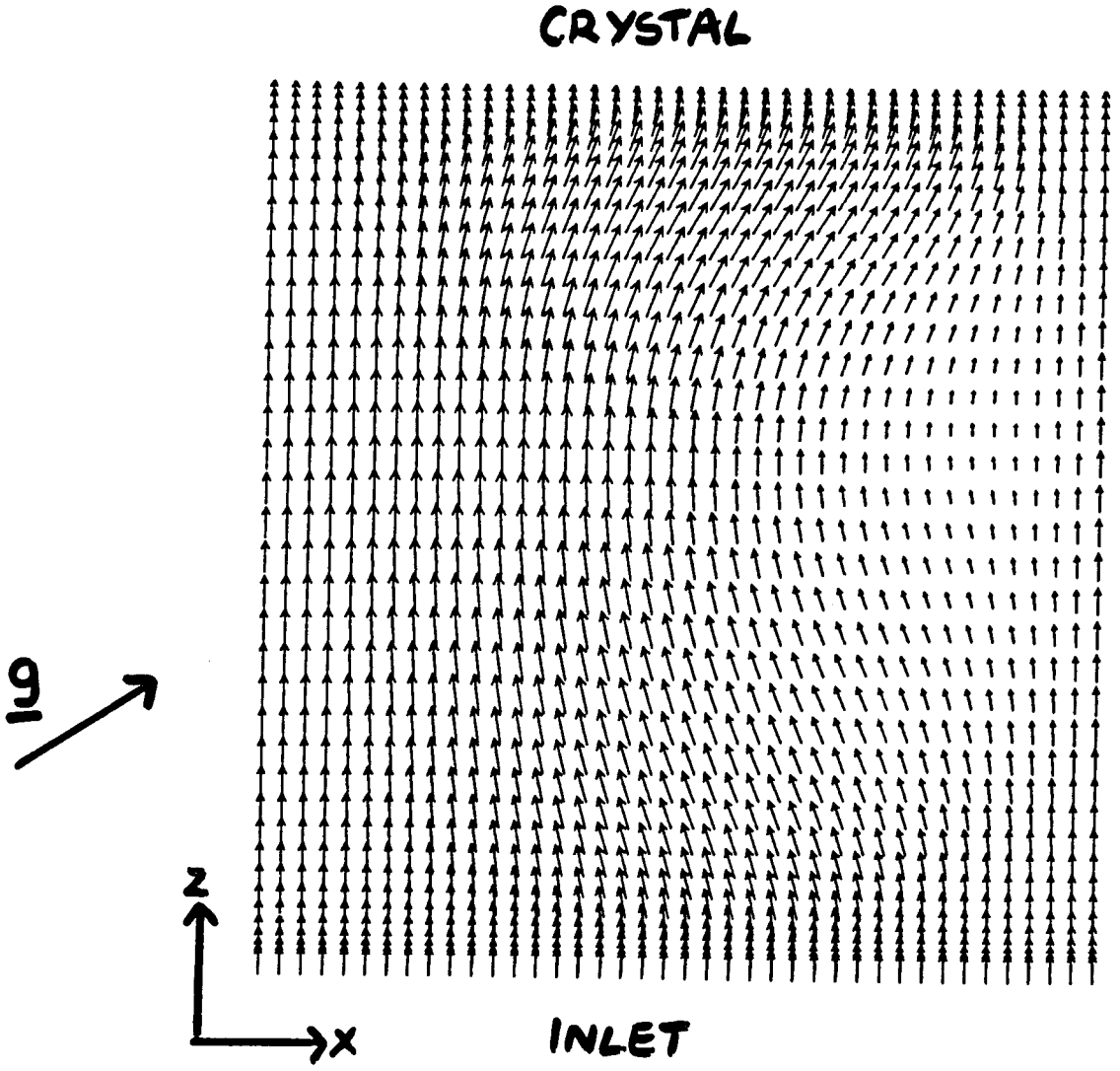

Figure 7. The steady flow field produced by a residual acceleration with a magnitude $5\sqrt{2}(10)^{-6}$ g acting at an angle of 45^{o} to the x-axis. The maximum speeds are approximately twice the growth speed, V_g = 6 μm s^{-1}.

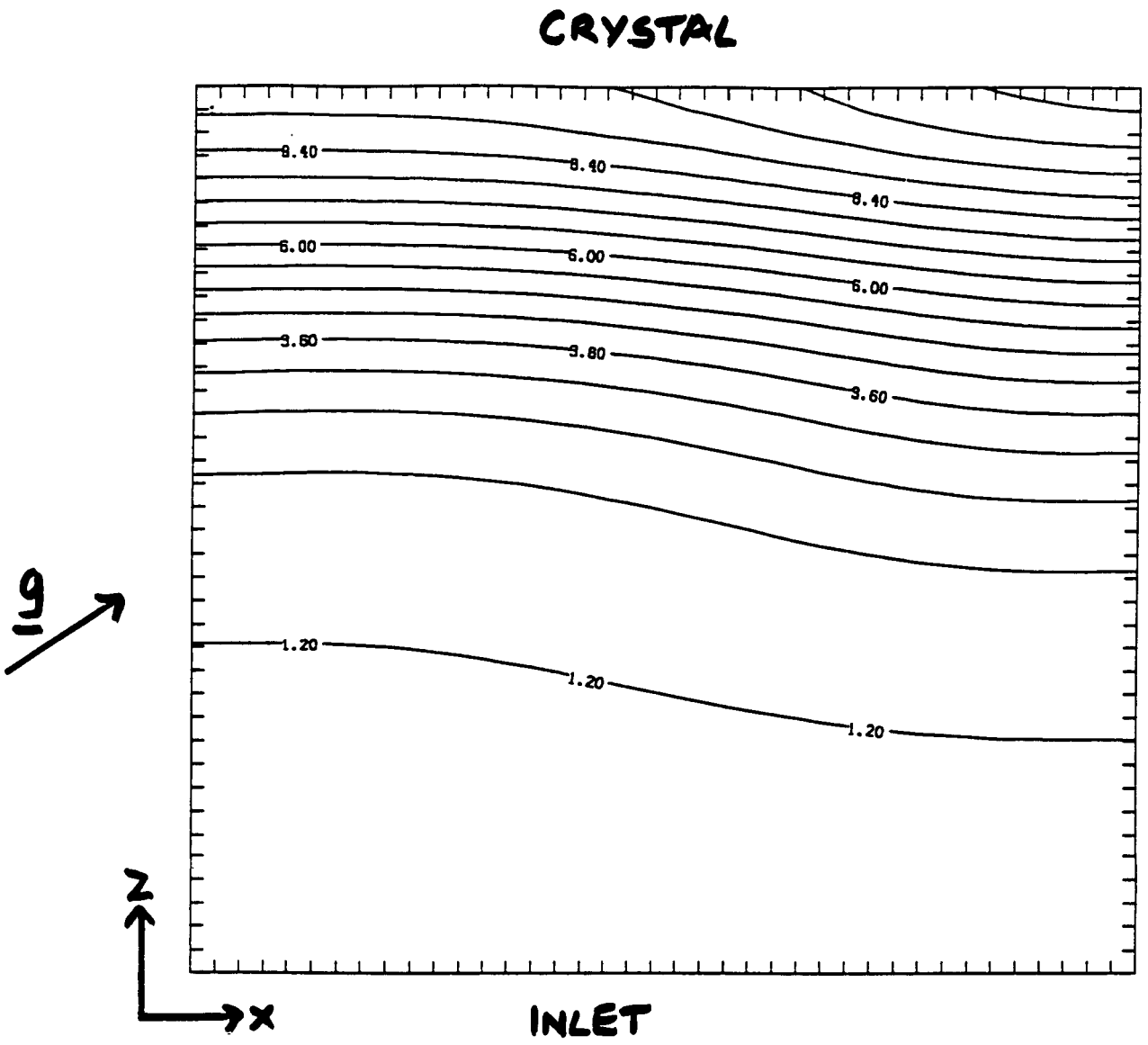

Figure 8. The solute field associated with the flow depicted in figure 7. For this case ξ= 57%.

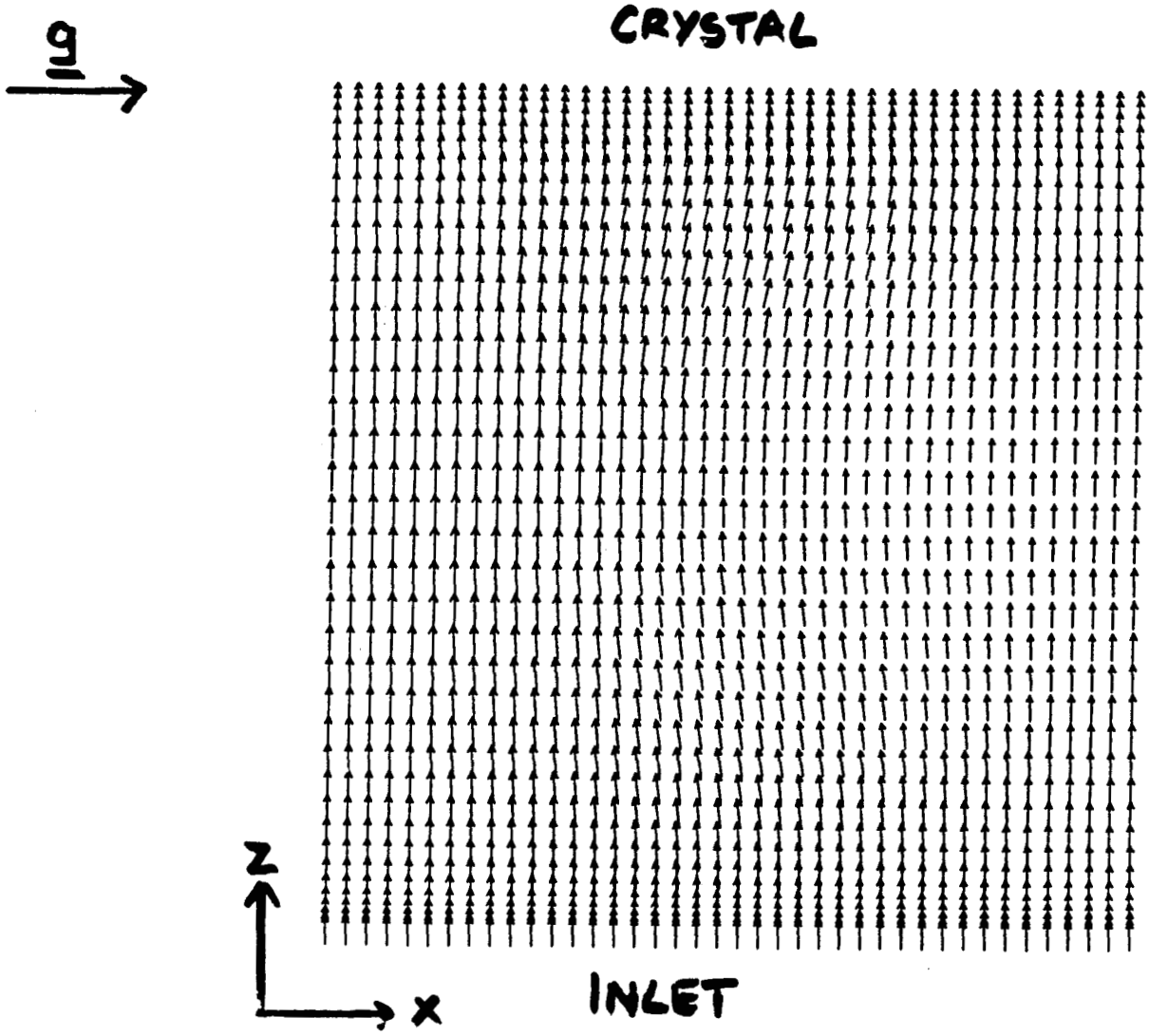

Figure 9 The steady flow field produced by a residual acceleration with a magnitude $\sqrt{2}(10)^{-6}$ g acting parallel to the crystal melt interface. The maximum speeds are only slightly higher than the growth speed, V_g = 6 μm s^{-1}.

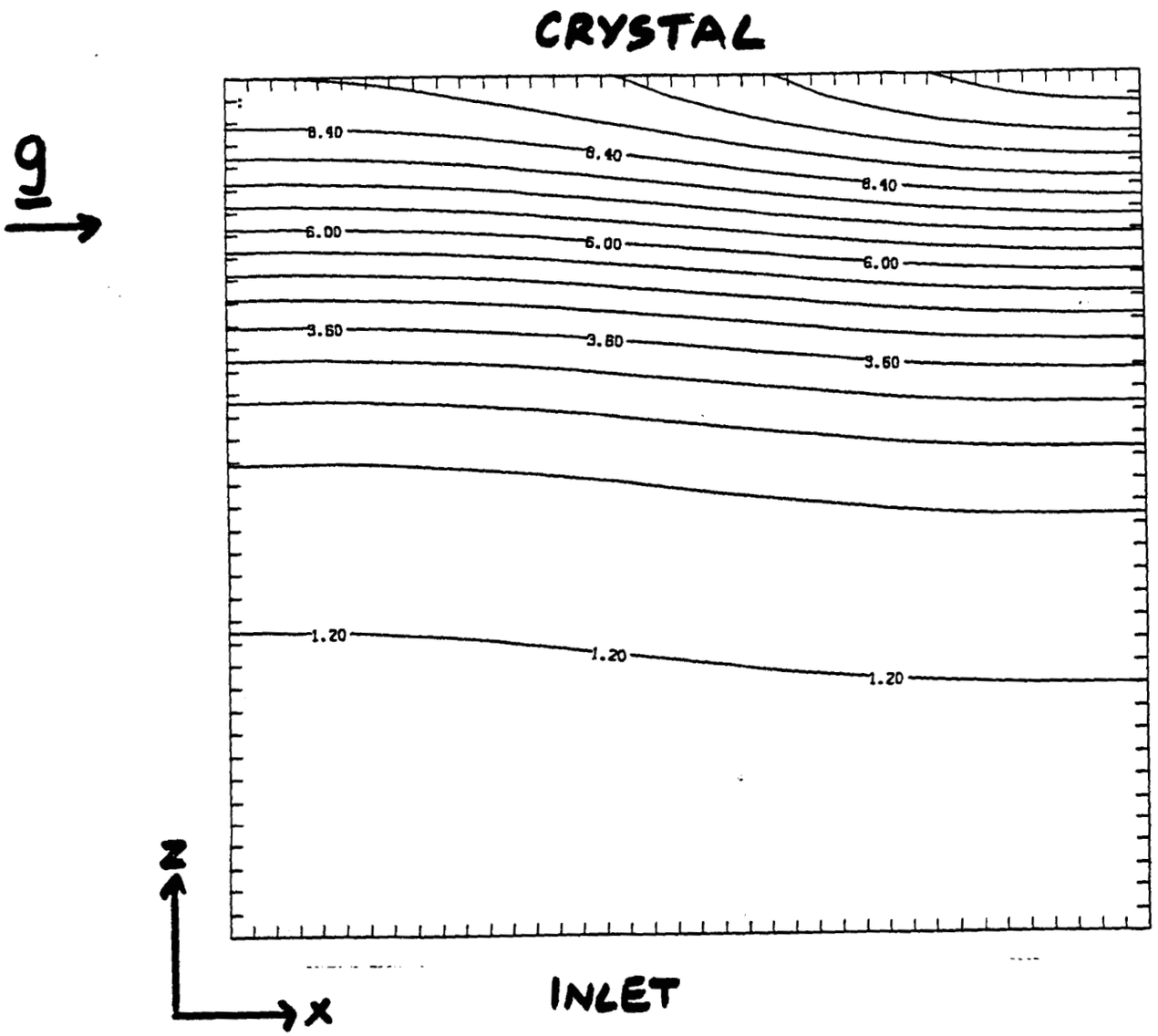

Figure 10. The solute field associated with the flow depicted in figure 9. For this case ξ= 22%.

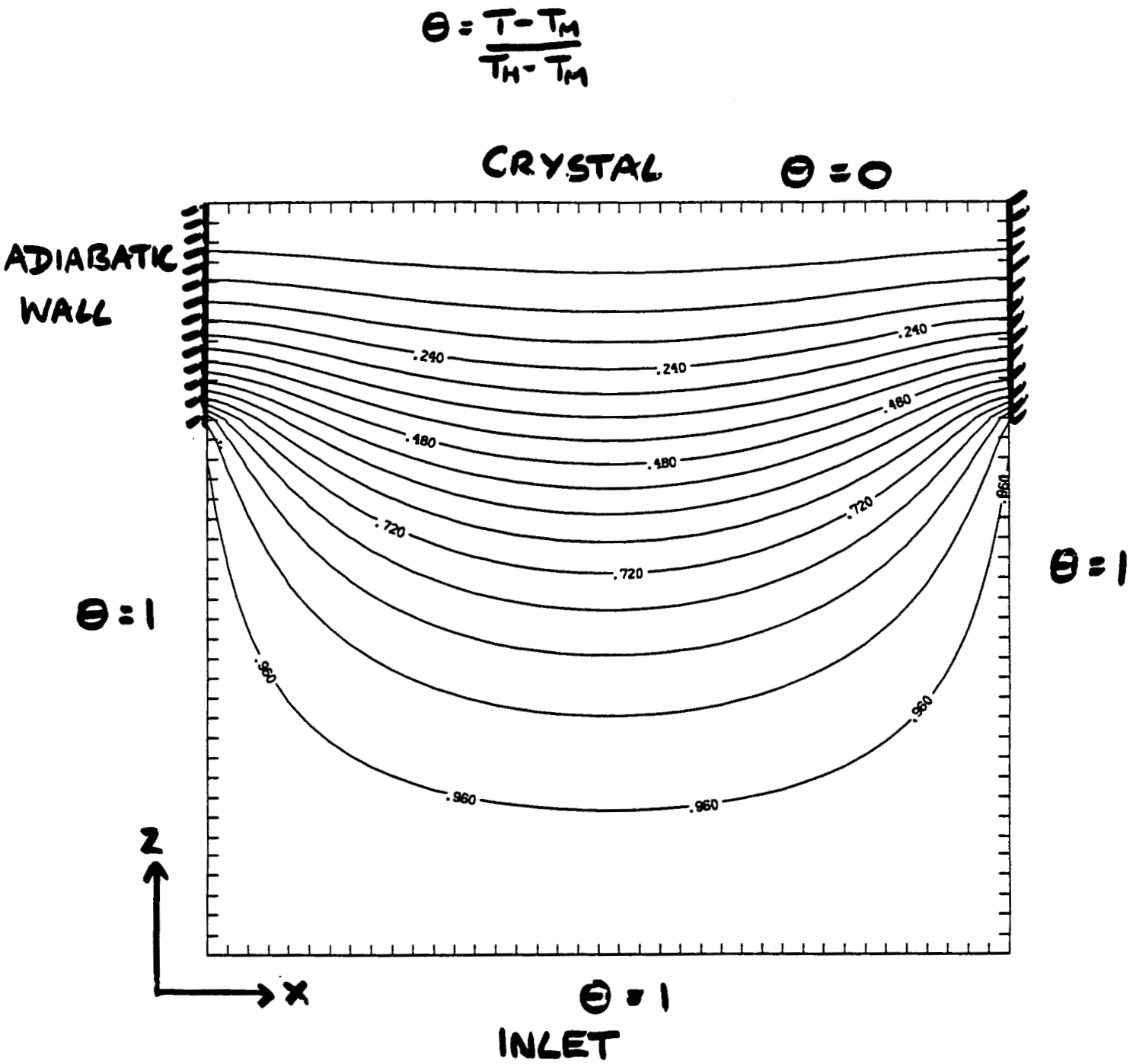

Figure 11. The temperature field for all 2-D cases discussed in this report.

2) Steady accelerations: 3-D

Five three-dimensional calculations were undertaken in order to calibrate our results, obtained using the code PHOENICS, against those of Chang and Brown [16] and also to examine the influence of a more realistic geometry. Three were axisymmetric with $\mathbf{g}_o$ anti-parallel to the solidification direction. Two were fully three-dimensional with $\mathbf{g}_o$ parallel to the crystal-melt interface. The compositional non-uniformity ξ was found to be approximately 10% lower for the axisymmetric cases than their 2-D analogs. These calculations were carried out for $||\mathbf{g}|| = 10^{-4}$, 10^{-3} and 10^{-2}. The fully 3-D cases were carried out for $||\mathbf{g}|| = \sqrt{2}(10)^{-5}$ and $\sqrt{2}(10)^{-6}$. At the higher value of the residual acceleration $\xi = 75\%$, approximately half the 2-D value. At $\sqrt{2}(10)^{-6}$ g, $\xi = 26\%$. Thus, for this case there was little difference between the 2 and 3-D predictions. Figures 12 and 13 depict the variation in solute concentration over the interface.

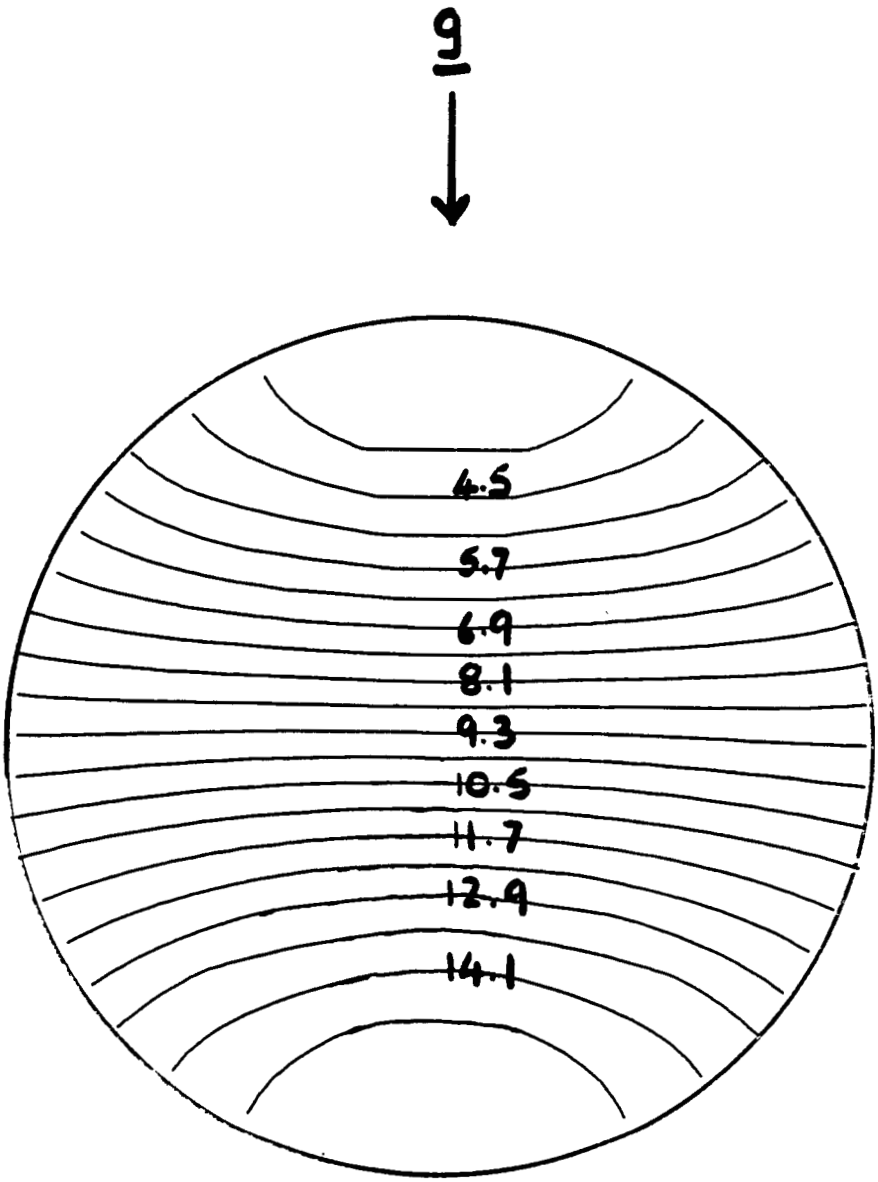

Figure 12. The steady solute distribution over the crystal-melt interface consequent to a $\sqrt{2}(10)^{-5}$ g acceleration oriented parallel to the interface.

ξ = 75%.

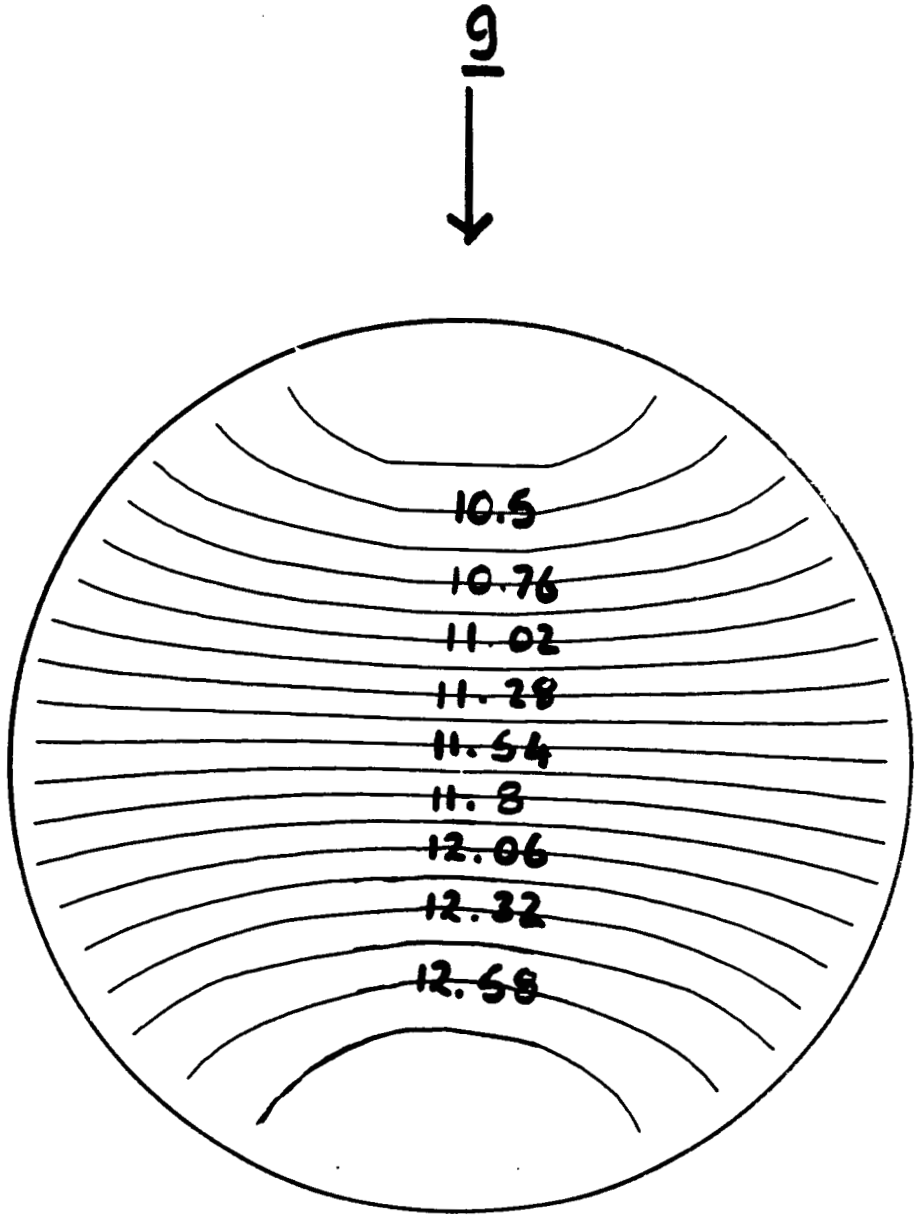

Figure 13. The steady solute distribution over the crystal-melt interface consequent to a $\sqrt{2}(10)^{-6}$ g acceleration oriented parallel to the interface.

$\xi = 26\%$.

3) Single frequency; combined steady + single frequency accelerations

A number of different types of periodic disturbances were examined. Single frequency disturbances of the form $\mathbf{g}(t) = \mathbf{g}_o + \mathbf{g}_n \cos(2\pi\omega_n t)$ were examined with $\mathbf{g}_o = 0$, $\sqrt{2}(10)^{-6}$ and $\sqrt{2}(10)^{-5}$, oriented parallel to, perpendicular to and at 45° to the crystal-melt interface. The range of frequencies examined was $\omega_n = 10^{-4}$, 10^{-3}, 10^{-2}, 10^{-1}, 1 and 10 Hz. For frequencies greater than 10^{-2} Hz, there were no discernable effects on the solute fields. The velocity field did, however, respond to the oscillatory disturbances. For the case of 10^{-3} Hz (at 5×10^{-6} g) the response of the solute field was significant. Lateral and longitudinal non-uniformity levels in excess of 15% were calculated. Figures 14 and 15 show the lateral non-uniformity as a function of time, and highlight the additive effects of steady and an oscillatory disturbance components.

4) **Multiple frequency accelerations**

Selected results showing the effects of multiple frequency disturbances are given in figures 16-19. The figures illustrate the response to a three component acceleration consisting of a steady and two periodic contributions: $\mathbf{g}(t) = \mathbf{g}_o + \mathbf{g}_1 \cos(2\pi 10^{-3}t) + \mathbf{g}_2 \cos(2\pi 10^{-2}t)$, where $||\mathbf{g}_o|| = \sqrt{2}(10)^{-6}$, $||\mathbf{g}_1|| = 3\sqrt{2}(10)^{-6}$ and $||\mathbf{g}_2|| = 3\sqrt{2}(10)^{-5}$; and a four component acceleration: $\mathbf{g}(t) = \mathbf{g}_o + \mathbf{g}_1 \cos(2\pi 10^{-3}t) + \mathbf{g}_2 \cos(2\pi 10^{-2}t) + \mathbf{g}_3 \cos(2\pi 10^{-1}t)$, where $||\mathbf{g}_o|| = \sqrt{2}(10)^{-6}$, $||\mathbf{g}_1|| = 3\sqrt{2}(10)^{-6}$, $||\mathbf{g}_2|| = 3\sqrt{2}(10)^{-5}$ and $||\mathbf{g}_3|| = 3\sqrt{2}(10)^{-4}$. The response is complex and is characterized by non-linear interaction between the components of the disturbance. Our results suggest that in general the response of a system to multiple frequency disturbances will be difficult to predict without specific analysis. A comparison between the two cases illustrated in figures 16-18 readily shows that the addition of the 10^{-1} Hz component to the 3-component disturbance drastically changes the nature of the velocity field and the time dependent behavior of the lateral non-uniformity.

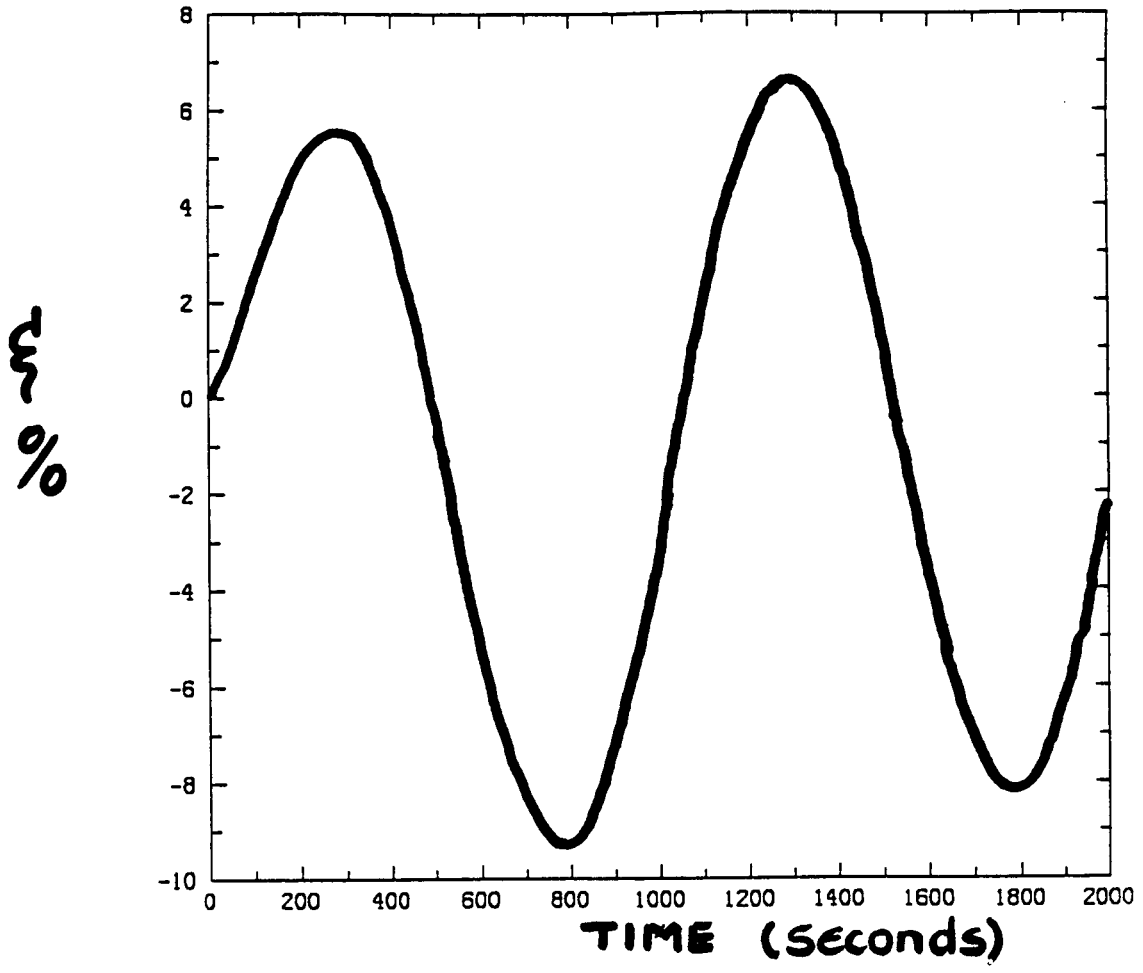

Figure 14. ξ plotted as a function of time for an oscillatory residual acceleration with a maximum magnitude of $3\sqrt{2}(10)^{-6}$ g and a frequency of 10^{-3} Hz, acting parallel to the crystal-melt interface.

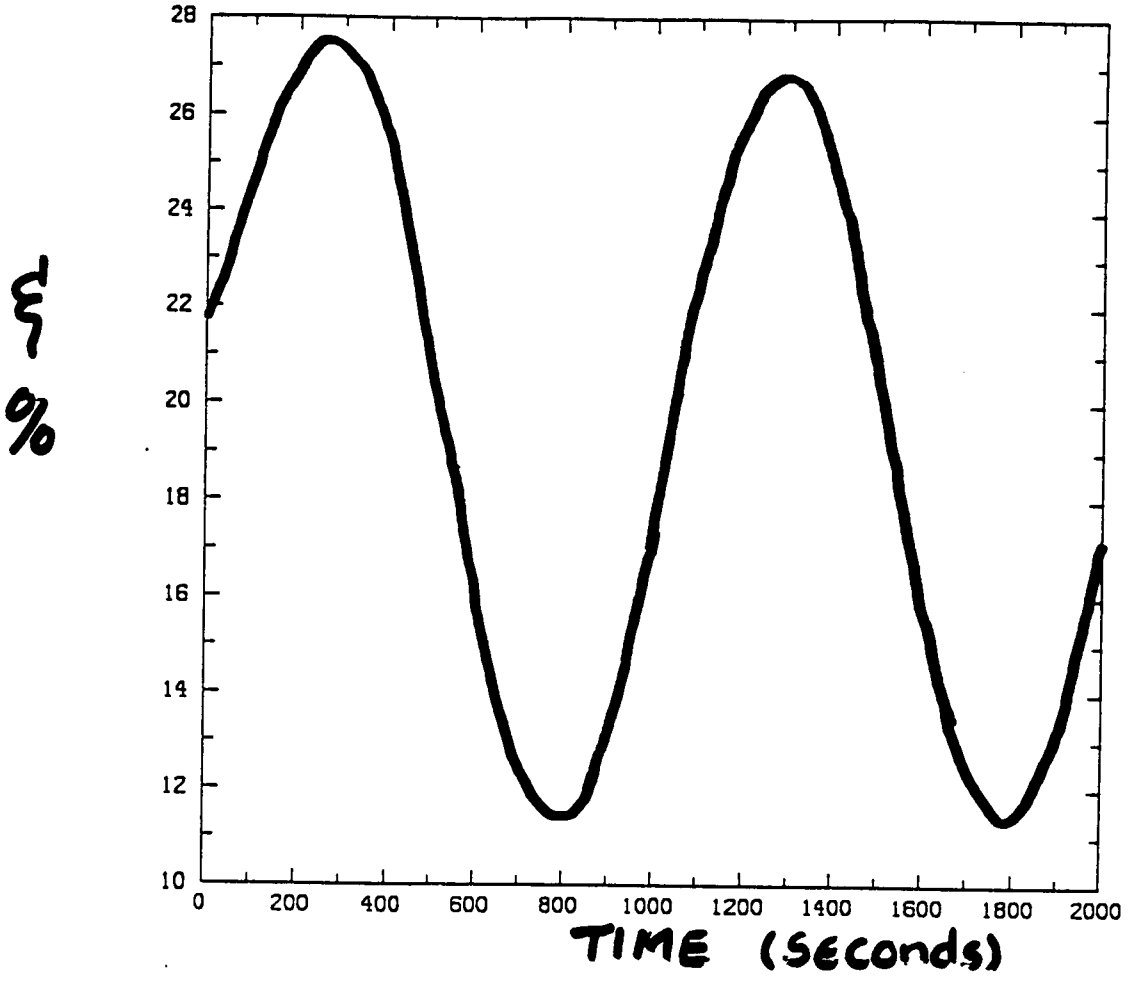

Figure 15. ξ plotted as a function of time for a residual acceleration consisting of a steady part with a magnitude of $\sqrt{2}(10)^{-6}$ g and an oscillatory part with a maximum magnitude of $3\sqrt{2}(10)^{-6}$ g and a frequency of 10^{-3} Hz, acting parallel to the crystal-melt interface.

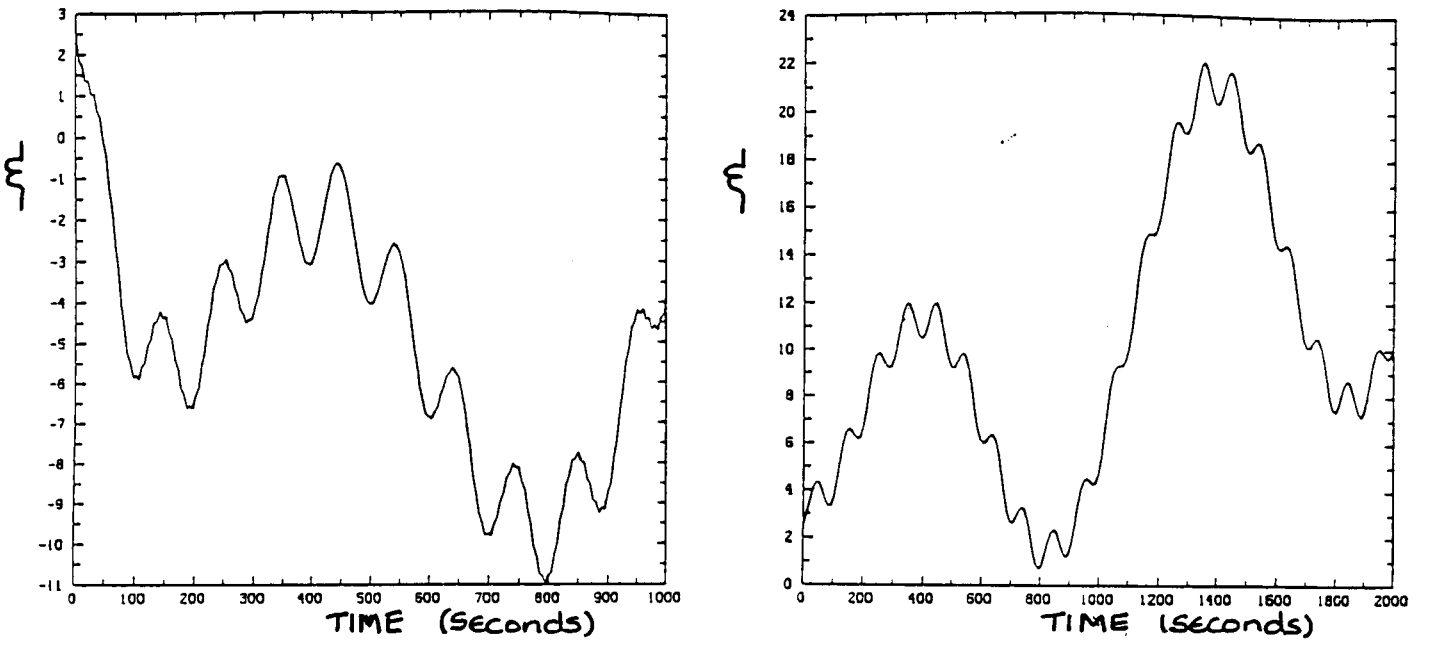

Figure 16. ξ plotted as a function of time for multi-component disturbances.

a) a steady low g background plus two periodic components:

$\mathbf{g}(t) = \mathbf{g}_o + \mathbf{g}_1 \cos(2\pi 10^{-3}t) + \mathbf{g}_2 \cos(2\pi 10^{-2}t)$, where $||\mathbf{g}_o|| = \sqrt{2}(10)^{-6}$, $||\mathbf{g}_1|| = 3\sqrt{2}(10)^{-6}$ and $||\mathbf{g}_2|| = 3\sqrt{2}(10)^{-5}$.

b) a steady low g background plus three periodic components:

$\mathbf{g}(t) = \mathbf{g}_o + \mathbf{g}_1 \cos(2\pi 10^{-3}t) + \mathbf{g}_2 \cos(2\pi 10^{-2}t)$ $+ \mathbf{g}_3 \cos(2\pi 10^{-1}t)$,

where $||\mathbf{g}_o|| = \sqrt{2}(10)^{-6}$, $||\mathbf{g}_1|| = 3\sqrt{2}(10)^{-6}$, $||\mathbf{g}_2|| = 3\sqrt{2}(10)^{-5}$ and $||\mathbf{g}_3|| = 3\sqrt{2}(10)^{-4}$.

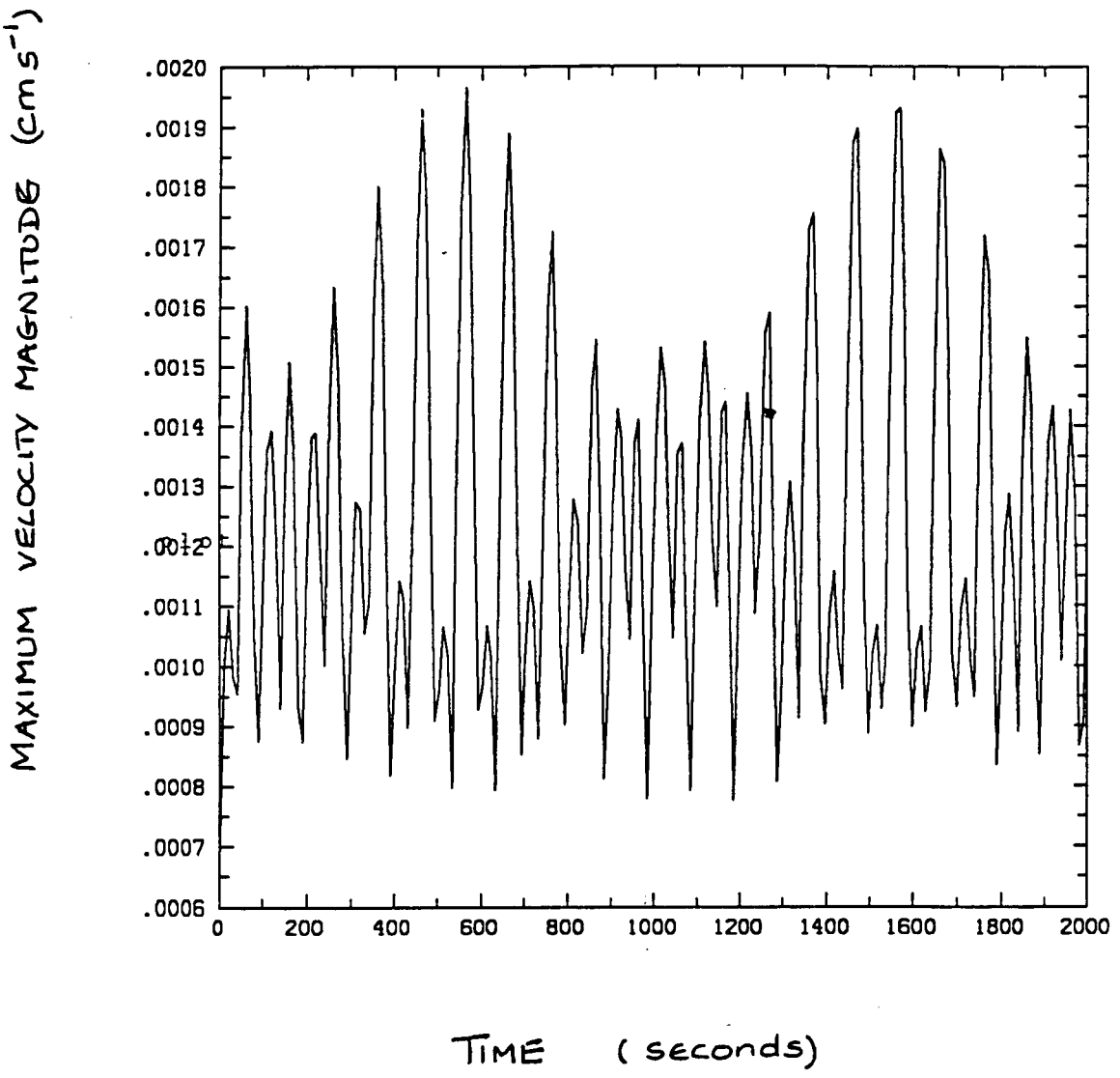

Figure 17. Maximum velocity as a function of time for the response to the multi-component disturbance of figure 16 a.

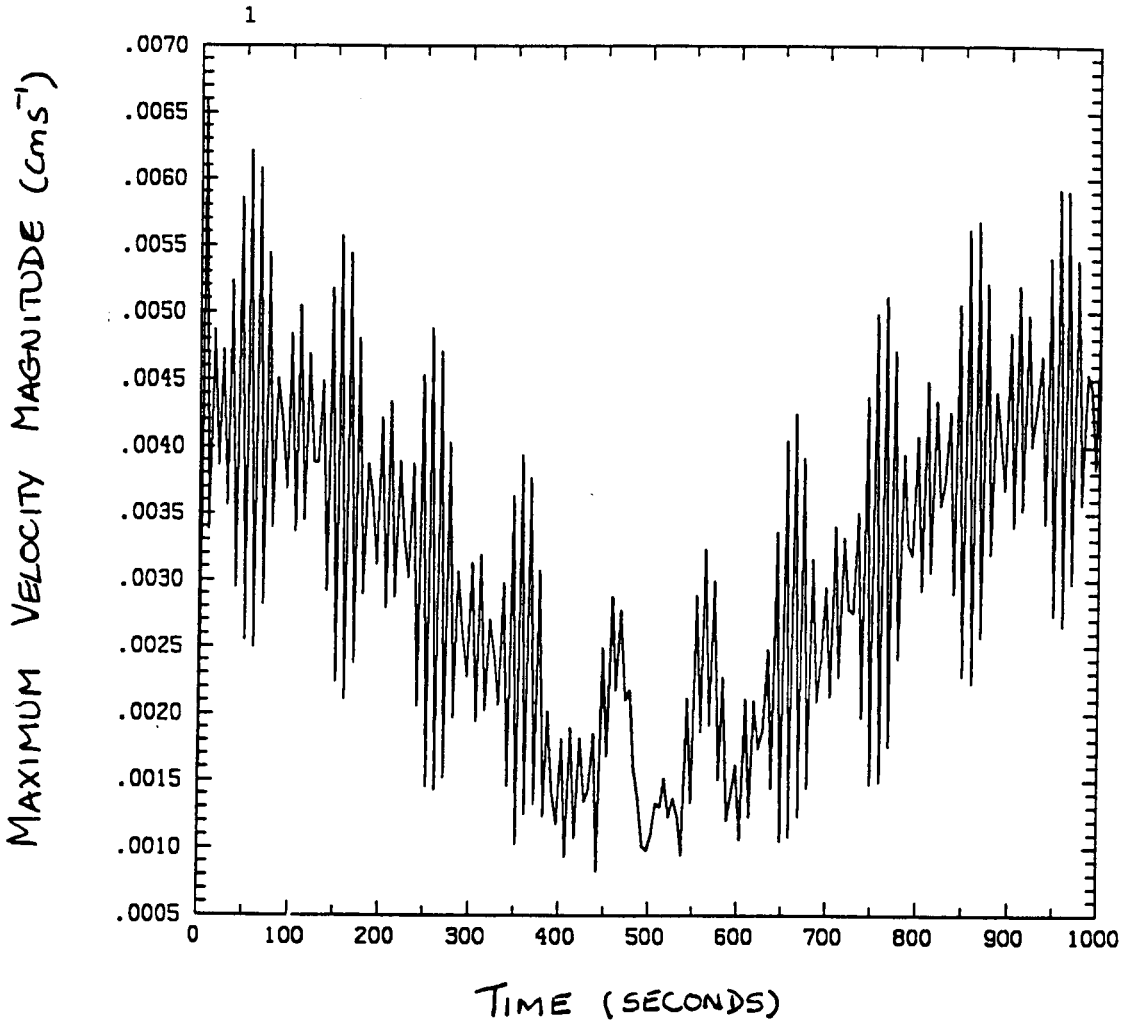

Figure 18. Maximum velocity as a function of time for the response to the multi-component disturbance of figure 16 b.

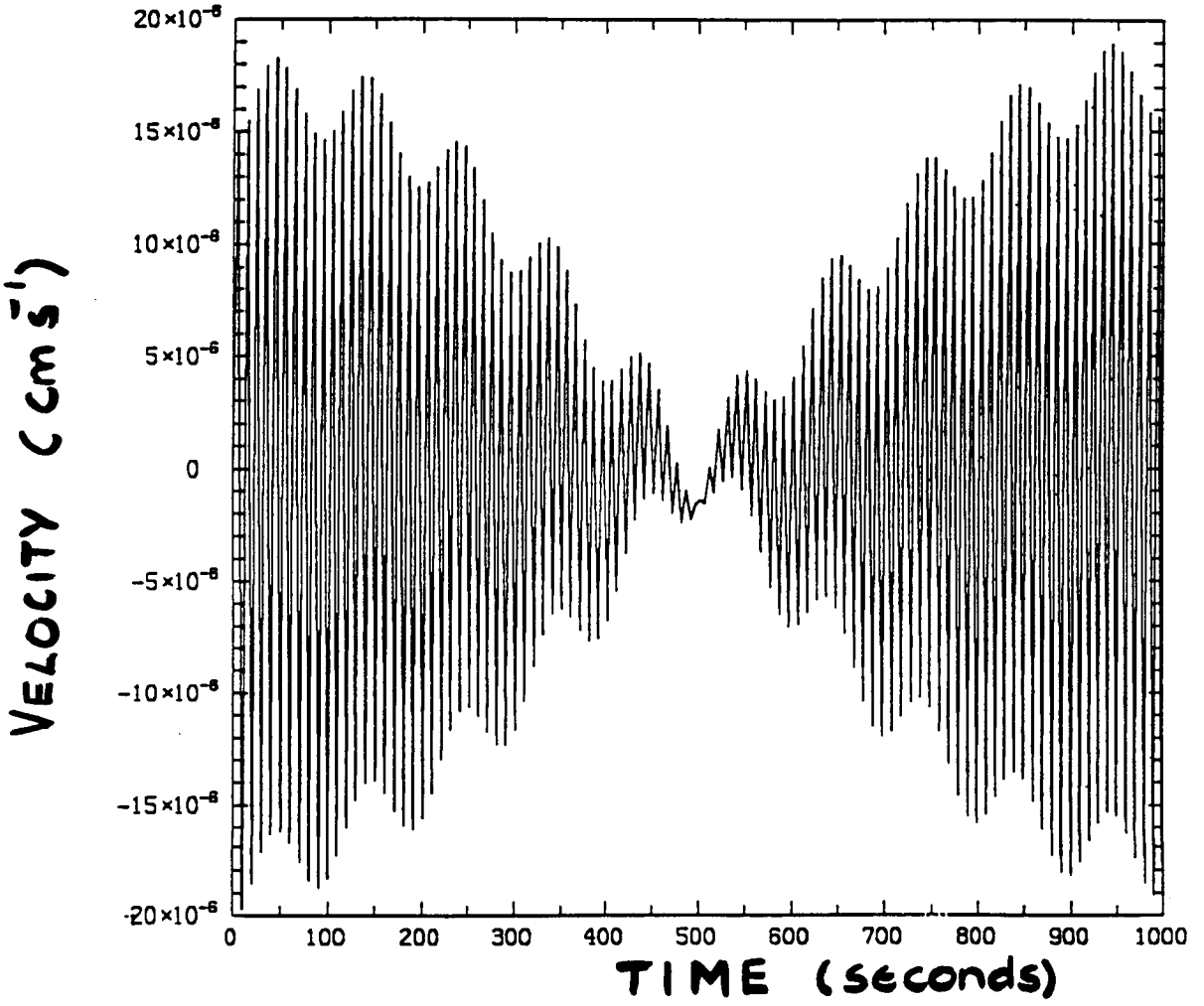

Figure 19. Response of a component of velocity to the multi-component disturbance of figure 16 b. at a selected point in the melt as a function of time. Note the characteristics of a combination resonant response.

5) Impulse-type accelerations

Four cases of impulse-type disturbances were examined. Of these the one second duration pulses had the most dramatic effects. Figure 20 depicts the flow field immediately after a one second $3x10^{-3}$ g impulse oriented parallel to the crystal interface. Figures 21-26 illustrate the development of the solute field following the impulse. The impulse has been superimposed onto a steady flow which is associated with a $\sqrt{2}(10)^{-6}$ g steady acceleration oriented anti-parallel to the impulse. Note that the effects are long lasting. The velocity field relaxes back to the initial state after some 300 seconds. The response of the solute field lags behind. The effect of the impulse is to initially reverse the flow field (compare figures 7 and 20). This has the effect of reducing the lateral compositional non-uniformity, eventually changing its sense. At approximately 260 seconds after the termination of the impulse the lateral segregation reaches a value of -26% whereupon it increases in value until it approaches its initial level of 21% after some 2000 seconds have elapsed.

A shorter duration (10^{-1} seconds) pulse resulted in a maximum deviation of the lateral non-uniformity of only 5% from the initial level after 350 seconds.

The effects of two one second pulses separated by one second were also calculated. The magnitude of the pulses was $3x10^{-3}$ g, and they were oriented parallel to the crystal interface. Their main effect was to drive the lateral segregation from 22% (the initial value) to -76% after 225 seconds.

So-called [5] "compensating" double pulses were also examined. A pulse anti-parallel to the background steady acceleration followed by an equal but opposite pulse does not result in a "null" effect. While the flow generated by the first pulse is reversed by the second pulse there is a net flow following the termination of the second pulse. This flow is in the same sense as the initial steady flow and results in an increase of the lateral non-uniformity in composition to a maximum of 24% at 100 seconds, whereupon it decays slowly to its initial value.

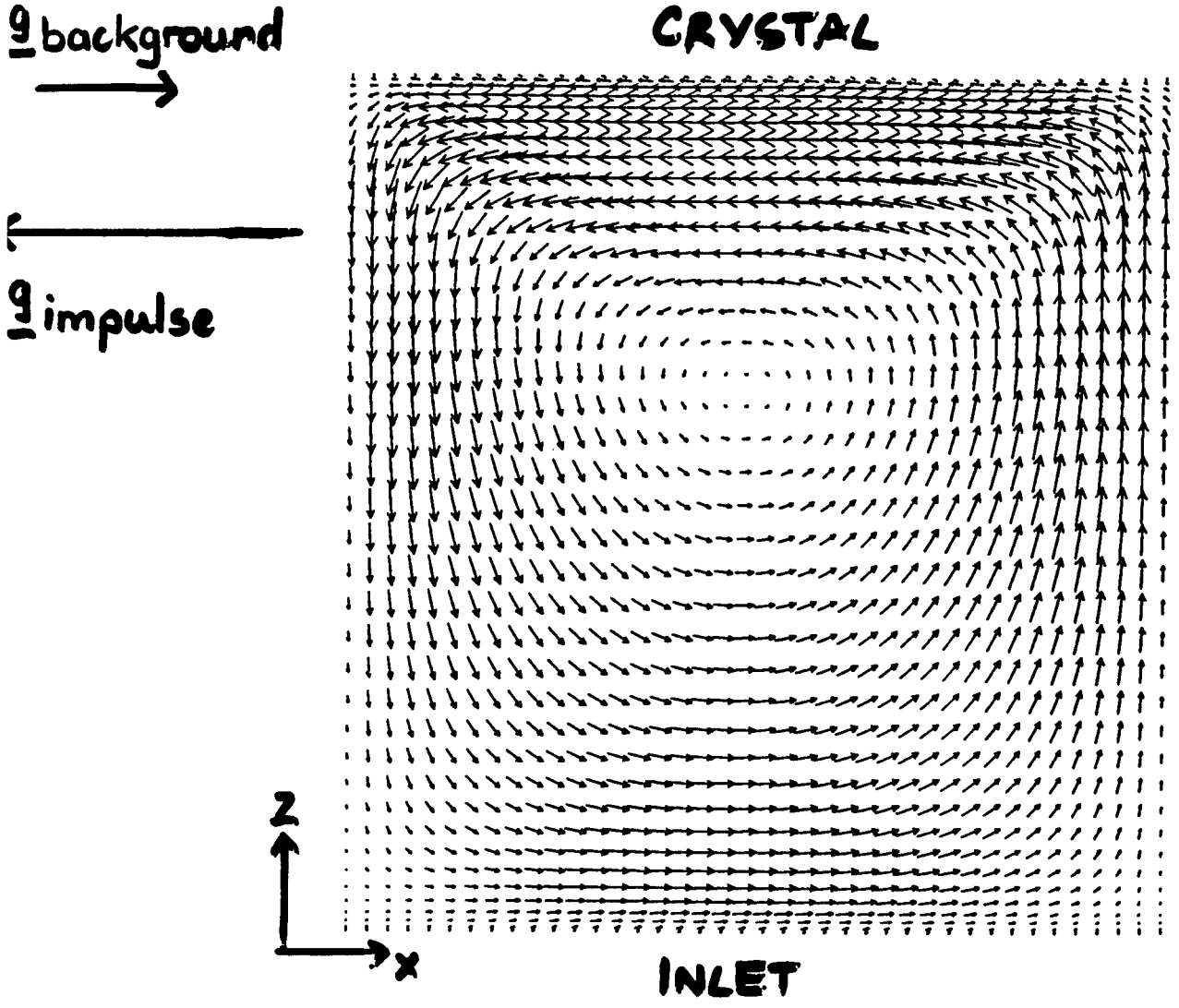

Figure 20. The velocity field after a one second pulse of $3(10)^{-3}$ g superimposed on a steady flow caused by a $\sqrt{2}(10)^{-6}$ g acceleration, both parallel to the crystal melt interface. The impulse is in the opposite direction to the background acceleration. Note that the maximum velocity magnitudes are of the order $3(10)^{-2}$ cm s^{-1} i.e. about 500 times the those of figure 9.

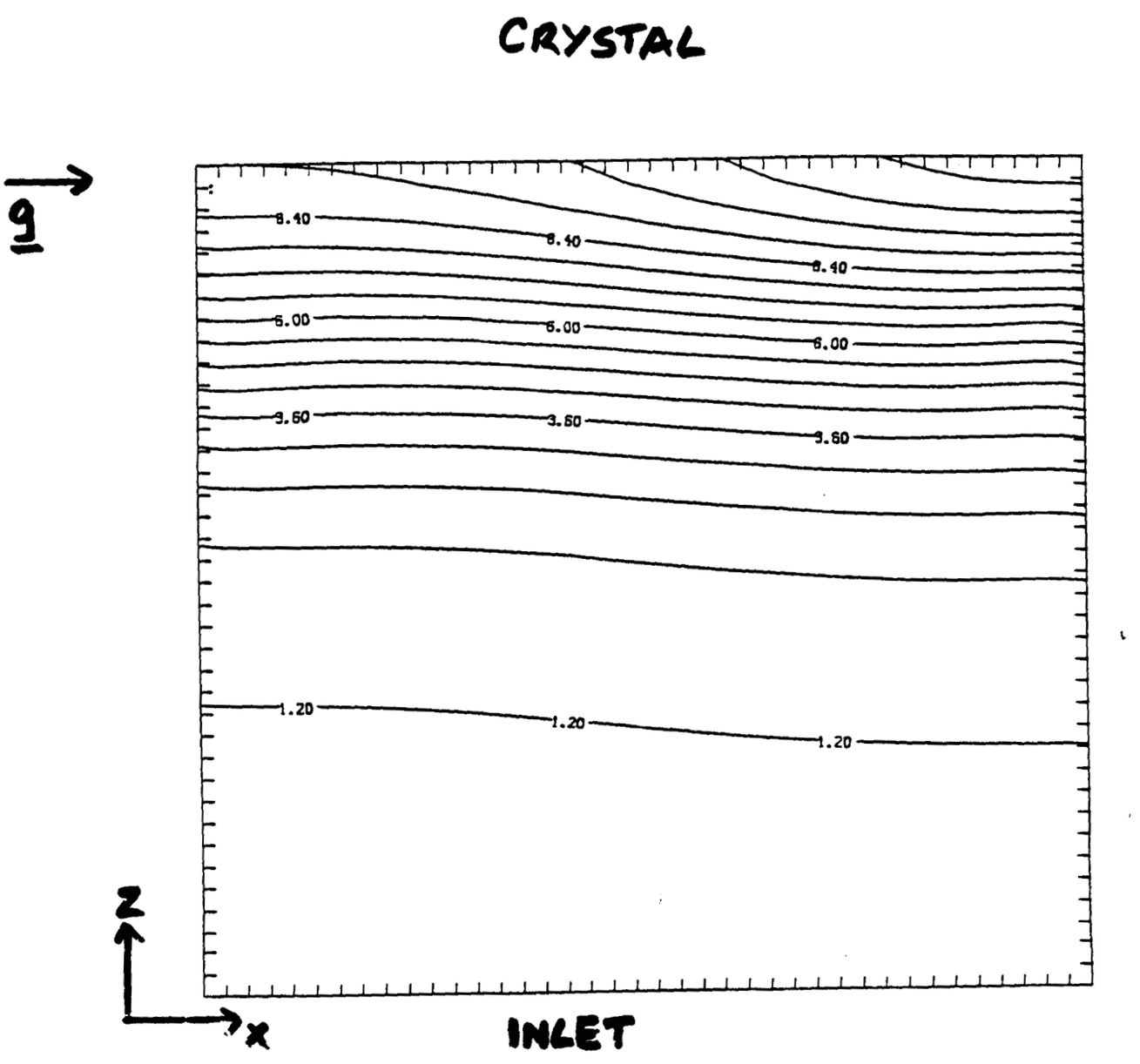

Figure 21. Solute field immediatley after the termination of the impulse.

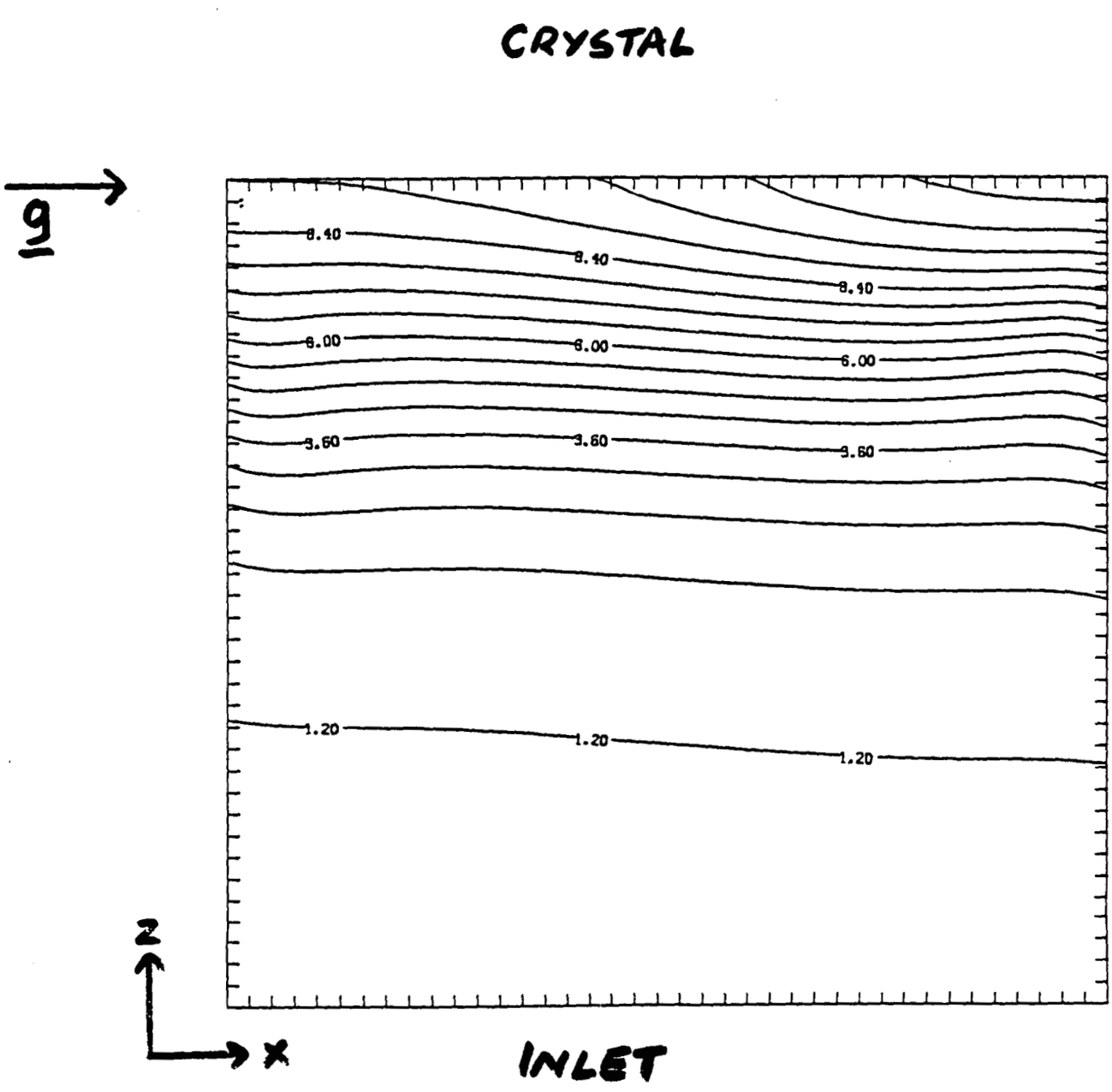

Figure 22. Solute field 31 seconds after the termination of the impulse.

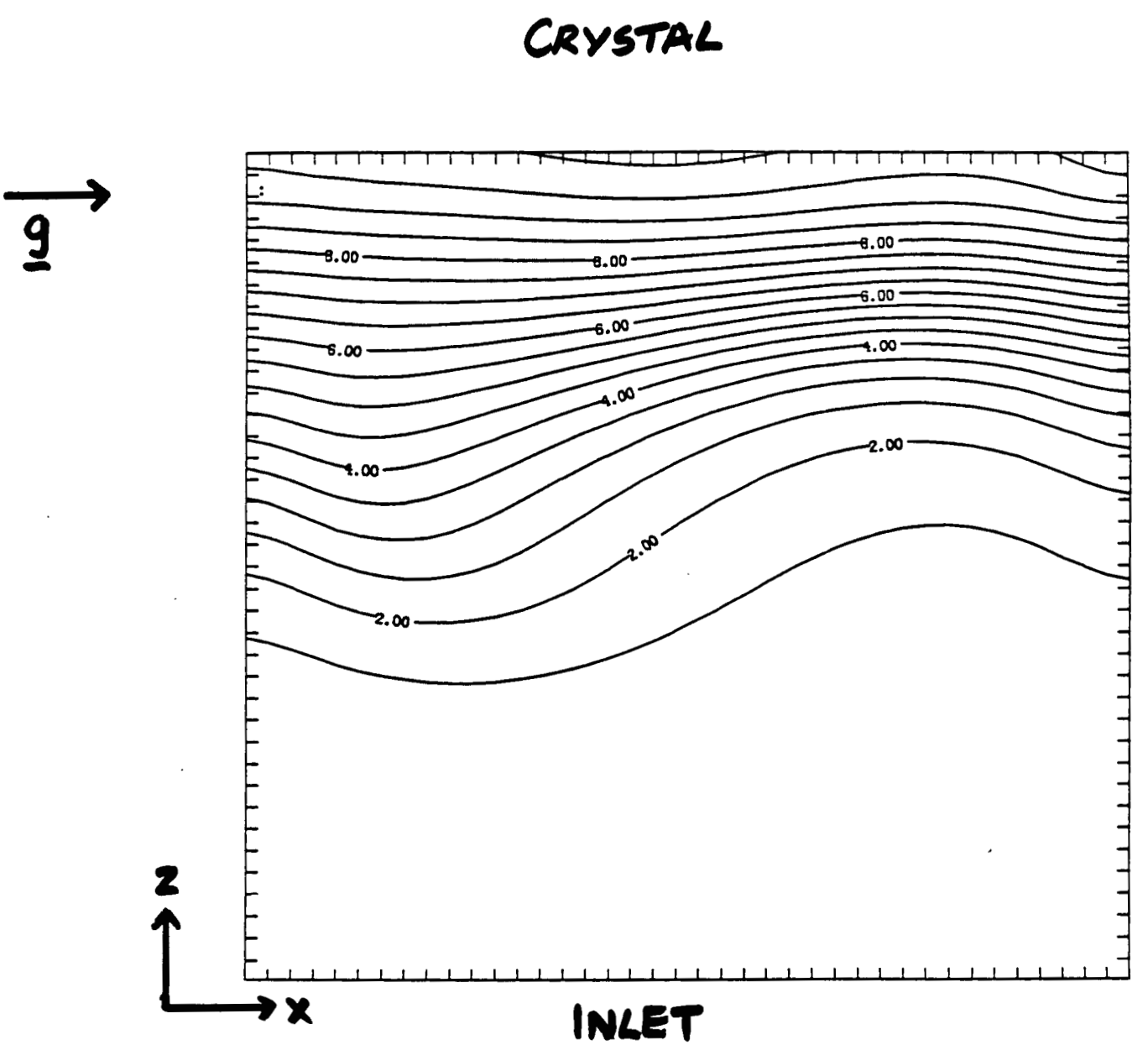

Figure 23. Solute field 81 seconds after the termination of the impulse.

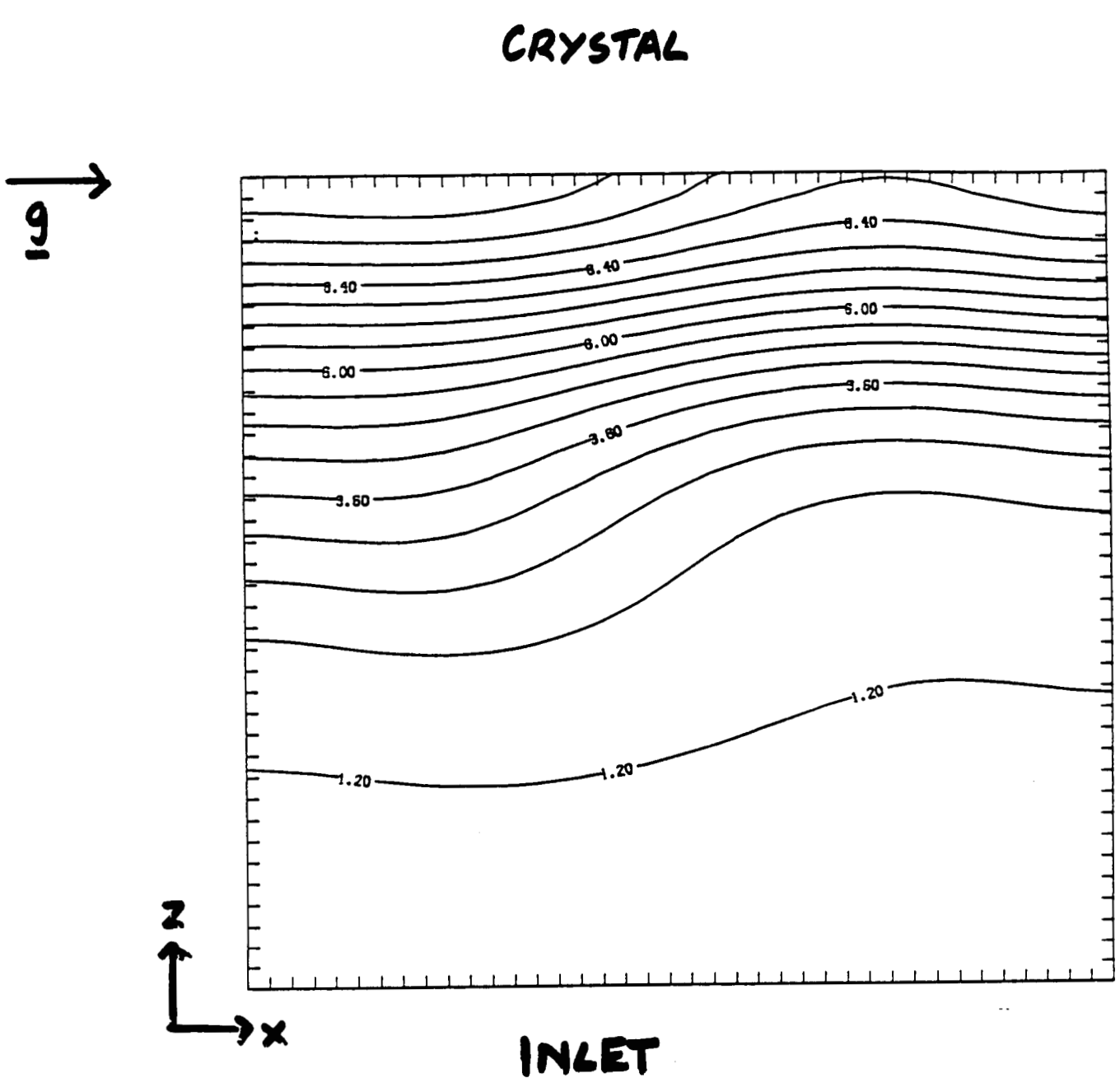

Figure 24. Solute field 431 seconds after the termination of the impulse.

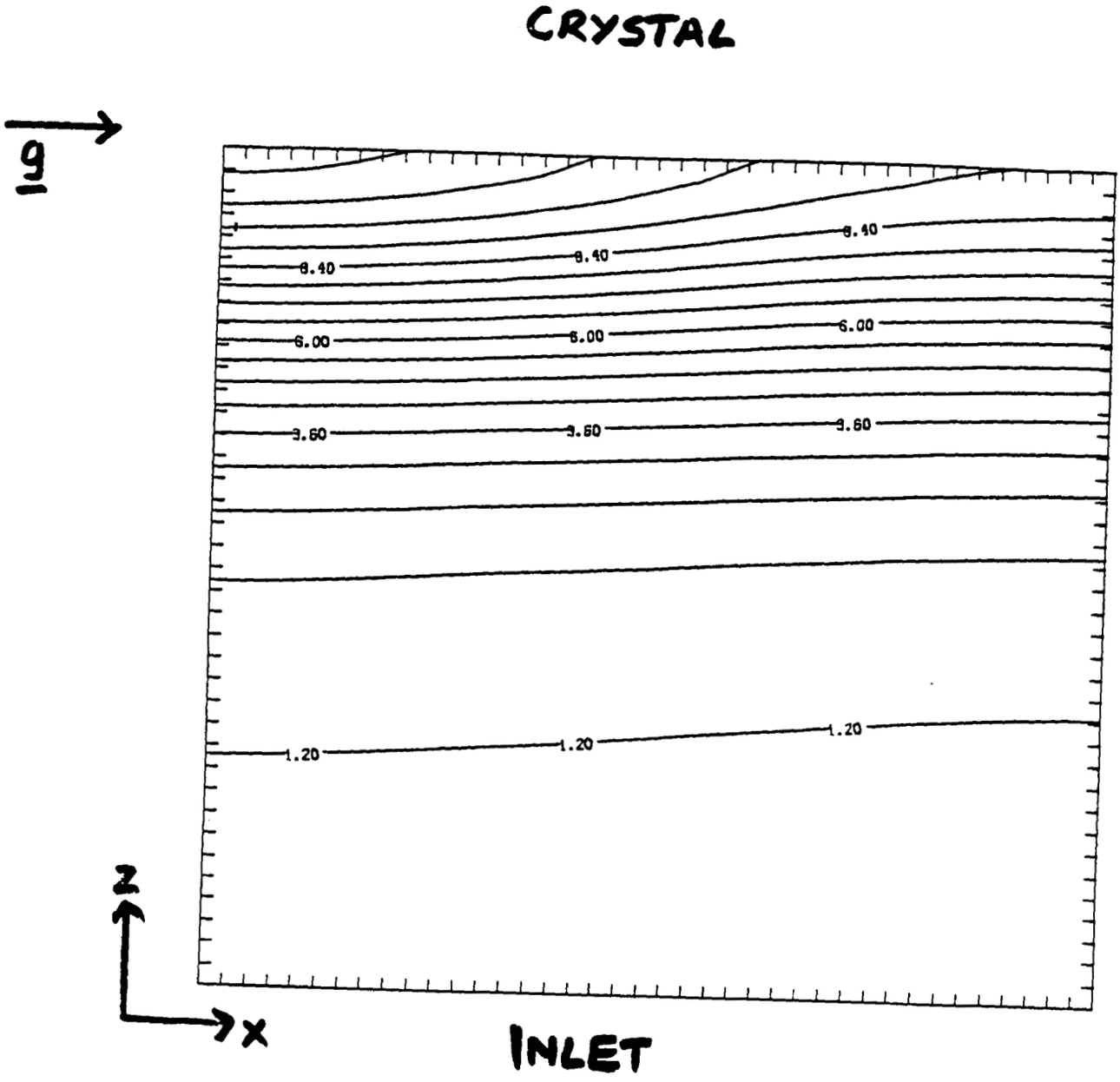

Figure 25. Solute field 881 seconds after the termination of the impulse.

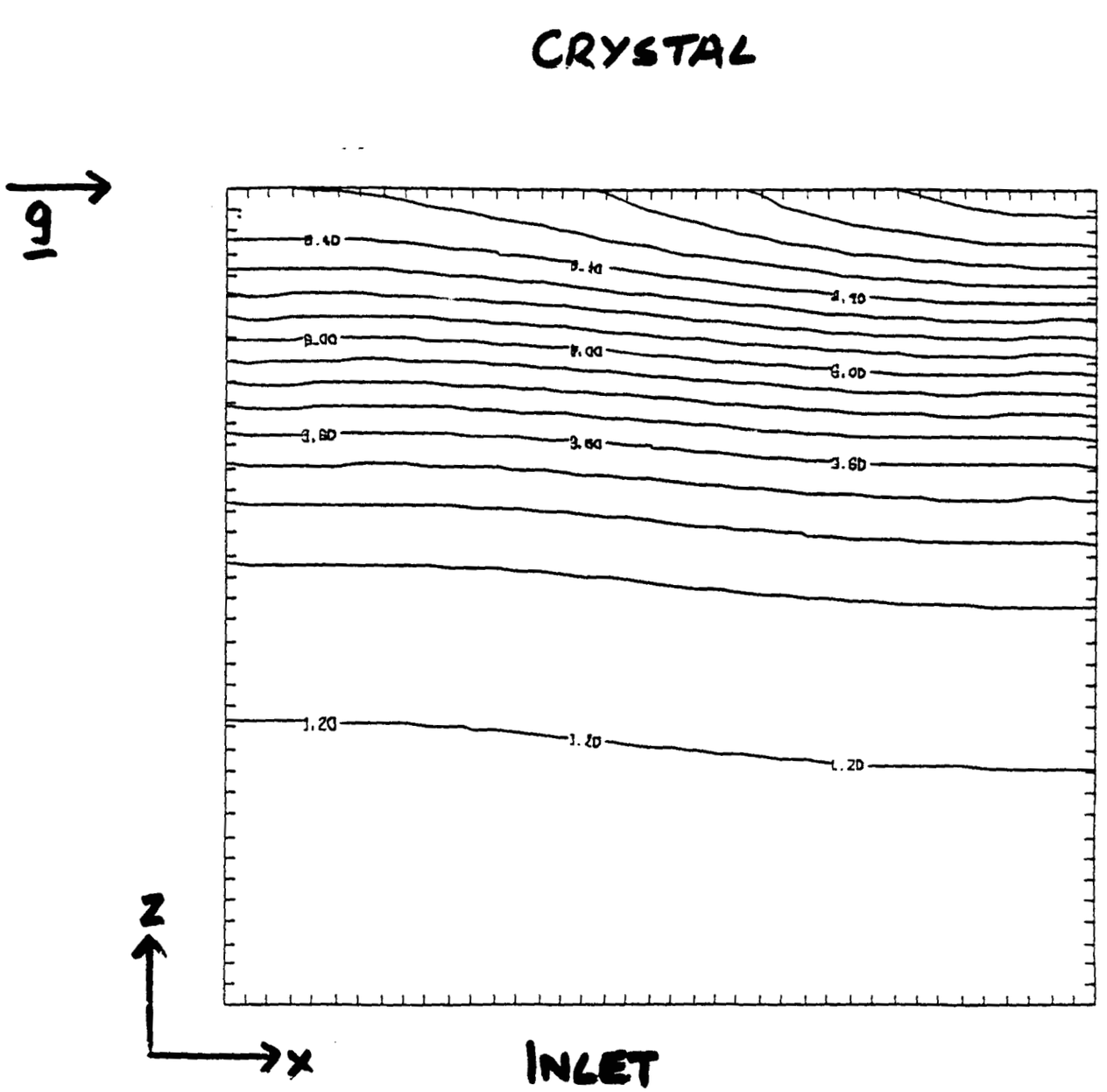

Figure 26. Solute field 1781 seconds after the termination of the impulse.

3.4 SUMMARY OF RESULTS FOR DIRECTIONAL SOLIDIFICATION

The salient results of our preliminary calculations for materials with properties and growth conditions similar to those listed in Table 2 can be summarized as follows:

1) A steady background level on the order of 10^{-6} - 10^{-5} g can be tolerated provided that the acceleration vector is *aligned with the axis of the growth ampoule*, and provided that no accelerations with frequencies less than 10^{-2} Hz (and amplitudes on the order of the steady component) are present.

2) For a fixed growth rate, the amount of lateral segregation is very sensitive to the orientation of the steady component of the residual gravity vector. The worst case appears to be when the acceleration vector is parallel to the crystal interface. At growth rates on the order of microns per second, this orientation can lead to non-uniformities of 22% when the magnitude of the acceleration is $\sqrt{2}(10)^{-6}$ g. If, however the growth rate is lowered by an order of magnitude, the non-uniformity is reduced significantly (down to 4-5% in this case).

3) The response of the solute field, and the lateral non-uniformity, to oscillatory accelerations varies from no response at all (at frequencies above 1 Hz with amplitudes below 10^{-3} g) to a significant response at 10^{-3} Hz at amplitudes on the order of 10^{-6} g. In addition, additive effects were observed for combinations of a steady component and a low frequency component. These additive effects gave rise to significant lateral and *longitudinal* non-uniformities in concentration.

4) A complicated non-linear response was observed for disturbances composed of a steady part and several frequencies. In one case that we examined, a component of the disturbance with a frequency of 10^{-1} Hz and a magnitude of 10^{-4} g appears to interact with lower frequency components to produce significant variations in the velocity and solute fields. In the absence of this 10^{-1} Hz disturbance the variations in the solute and velocity fields are still considerable but have a very different character. Owing to the non-linearities it is difficult to draw any general conclusions regarding the nature of the response to multiple frequency disturbances. We conjecture however that the response of the velocity depicted in figure 19 is due to a combination resonance [24]. This is justifiable if one considers that the temperature field is insensitive to the

flow, and is independent of time. Thus, the buoyancy term in the momentum equation (1) acts like a forcing function rather than a non-constant coefficient preceding a dependent variable. Had the temperature field been time-dependent the resonance could still arise. Although in this instance parametric excitation [24,25] can also play a role and the types of resonance possible would include primary, secondary, and combination resonances, as well as saturation and non-existence of periodic response [24].

5) The effects of impulse-type disturbances can be severe and can extend for a long time ($1\text{-}2\text{x}10^3$ seconds) after the termination of the impulse. The nature of the response depends on the magnitude, direction and duration of the impulse, and whether sequential opposing impulses are involved. A so-called "compensating" double pulse will not always result in offsetting effects.

A pulse with a one second duration, or a combination of such pulses has a drastic effect on the segregation levels at pulse amplitudes of 10^{-3} g. Impulses appear to have important consequences for the transient behavior of growth systems in general.

It should be borne in mind that our calculations have only covered a small part of a large parameter space. In particular it should be noted that for a given level of residual acceleration the amount of lateral segregation can be expected to increase with increasing Schmidt number and with decreasing distribution coefficient k [16,26]. We have also examined the effect of the growth rate and have found that a reduction in growth rate by an order of magnitude will result in a reduction in non-uniformity (for the range of parameters we have studied). This is consistent with the results of Adornato and Brown [26]. The consequences of variations in these parameters in relation to the type of time dependent accelerations dealt with in this preliminary communication will be investigated as part of the ongoing research program at the CMMR.

4. THERMAL CONVECTION IN A SQUARE CAVITY

This work was carried out in order to investigate the reliability of order of magnitude estimates of the affects of residual accelerations on transport conditions in simple fluid systems.

The chosen systems involved thermal convection in square and rectangular cavities. The rigid upper and lower boundaries were maintained at constant but different temperatures. The temperature differences examined ranged from 5 K to 50 K over 1-5 cm. The sidewalls were insulating. The applied residual gravity vector was time dependent in both magnitude and orientation. A variety of accelerations were examined with forms similar to those listed in Table 3. It became readily apparent that while the fluid responded to the body force, the temperature field was relatively insensitive. At Prandtl numbers of order one the temperature field exhibited minor oscillations about the basic diffusion profile (a simple linear profile for this case). However, none of the cases examined showed a significant fluctuation in heat flux at the low temperature boundary. The major reason for this appears to be the strong influence of our thermal boundary conditions on the heat transfer rates in the system.

In order to test the reliability of order of magnitude estimates the g-sensitivity predicted by the Langbein-Tiby approach was also tested. The basic scenario is that described in their paper [6]. " *In many fluid physics experiments, when particle motion is observed or the behaviour of a growth front is studied, one can assume that* $\delta\rho/\rho$ [the average density change] *in the test volume has the order of magnitude* 10^{-2} *. ..the diameter of the test volume is chosen to be 2 cm, temperature differences of 5 K are applied and an accuracy of* $\delta T = 0.05$ *K is required ...*" In addition we assumed adiabatic sidewalls.

The estimated tolerable g-level for the the above requirement is given as

$$a_{max} = 2[\ \omega^2 + (\nu/\ L^2\ )^2]^{1/2}\ [\ \omega^2 + (\kappa/\ L^2\ )^2]^{1/2},$$

and is based on a "typical velocity" magnitude of [6]

$$O\ [\ \mathbf{u}(\mathbf{r})] = (\delta\rho/\rho)\ a_o\ \omega^{-1}[\ \omega^2 + (\nu/\ L^2\ )^2]^{-1/2}\ ,$$

where ω is the frequency of the residual acceleration, $\nu = 10^{-2}\text{cm}^2\ \text{s}^{-1}$ is the kinematic viscosity of the fluid, $\kappa = 10^{-2}\text{cm}^2\ \text{s}^{-1}$ is the thermal diffusivity, L is the characteristic length (taken to be 2 cm) and a_o is the

magnitude of the acceleration. The predicted order of magnitude of **u** for a steady acceleration of 10^{-6} g is which is three orders of magnitude higher than the maximum velocity computed from the solution of the full non-linear equations. In every case we examined, the maximum velocity estimates were at least two to three orders of magnitude higher than our maximum computed velocities. As a consequence, the effect of residual accelerations tend to be over estimated. These discrepancies can be explained simply in terms of lack of a suitable length scale on which to base the estimates and the fact that order of magnitude estimates cannot, in general, properly account for the geometrical and thermal nature of the boundary conditions.

5. REFERENCES

[1] R. P. Chassay and A. J. Schwaniger, Jr., NASA -TM 86585, December, 1986.

[2] H. Hamacher, R. Jilg, U. Mehrbold, Proc. 6th European Symposium Materials Sciences in Microgravity Conditions, Bordeaux, France (ESA SP-256 1987).

[3] Y. Kamotani, A. Prasad and S. Ostrach, AIAA Journal 19 (1981) 511.

[4] G. B. McFadden and S. R. Coriell, to appear in Proc. 1st National Fluid Dynamics Congress, Cincinnati, July 1988.

[5] R. Monti, ESA Contract Report, R-66.525, Technosystems Report TS-7-87, April 1987.

[6] D. Langbein and C. Tiby, ESA Contract Report No. 5.504/83/F/FS(SC, Battelle, Frankfurt 1983.

[7] D. Camel, J.J. Favier and A, Rouzaud, ESA Contract Report, Gr-764.108, March 27 1987.

[8] S. Ostrach, in Materials Processing in Space: A Workshop, ed. S. Ramascskan (Indian Acad. Sci. Bangalore 1982).

[9] R. Monti, J.J. Favier and D. Langbein, in Fluid Sciences and Materials Science in Space, A European Perspective, Ed. H. U. Walter (Springer, Berlin 1987) p. 637.

[10] A. Rouzaud, D. Camel and J.J. Favier, J. Crystal Growth 73 (1985) 149.

[11] R. Naumann, personal communication, March 1988.

[12] R. Monti and L. Napolitano, Technosystems Report TS-7-84, June 1984.

[13] D. Camel and J.J. Favier, J. Crystal Growth 67 (1984) 42.

[14] D. Camel and J.J. Favier, J. Crystal Growth 73 (1984) 57.

[15] D. Camel and J.J. Favier, J. de Physique 47 (1986) 1001.

[16] C.J. Chang and R.A. Brown, J. Crystal Growth 63 (1983) 343.

[17] M. D. Radcliffe, M. C. Drake, G. Zvan, W. W. Fowlis, J. I. D. Alexander, G. D. Roberts, J. K. Sutter and E. Bergman, in Proceedings of the American Chemical Society Meeting, New Orleans 1987.

[18] S. J. Robertson and L. A. Nicholson, Lockheed Report LMSC-HREC TR D867640 September 1987.

[19] S. J. Robertson, L. A. Nicholson and L. W. Spradley, Lockheed Report LMSC-HREC TR D867624 September 1982.

[20] L. W. Spradley, S. W. Bourgeois and F. N. Lin, AIAA paper 75-695, 1975.

[21] S. Weinbaum, J. Fluid Mech. 18 (1964) 409.

[22] A.P. Goshman and W. M. Pun, Report No. HTS (74) 2, (Imperial College London U.K. 1973).

[23] S. V. Patankar, Numerical Heat Transfer and Fluid Flow (Hemisphere Publishing Co., New York 1980).

[24] A. H. Nayfeh and D. T. Mook Nonlinear Oscillations, (Wiley, New York 1979).

[25] G. Z. Gershuni and E. M. Zhukovitskii, Convective Stability of Incompressible Fluids, (Israel Program for Scientific Translations, Jerusalem 1976).

[26] P. M. Adornato and R. A. Brown, J. Crystal Growth 80 (1987) 155-190.